symmetry

MDPI

Article

From Symmetry to Asymmetry: The Use of Additional Pulses to Improve Protection against Ultrashort Pulses Based on Modal Filtration

Anton O. Belousov, Evgeniya B. Chernikova *, Mariya A. Samoylichenko, Artem V. Medvedev, Alexander V. Nosov, Talgat R. Gazizov and Alexander M. Zabolotsky

Tomsk State University of Control Systems and Radioelectronics, 634050 Tomsk, Russia; ant1lafleur@gmail.com (A.O.B.); 1993mary2011@mail.ru (M.A.S.); medart20@rambler.ru (A.V.M.); alexns2094@gmail.com (A.V.N.); talgat@tu.tusur.ru (T.R.G.); zabolotsky_am@mail.ru (A.M.Z.)

* Correspondence: chiernikova96@mail.ru; Tel.: +7-(923)-407-47-23

Received: 30 May 2020; Accepted: 3 July 2020; Published: 5 July 2020

Abstract: For the first time, the paper considers in a unified work the possibility of the appearance of additional pulses in various structures based on modal filtration technology, which is used to improve protection against ultrashort pulses (USP). We analyzed meander lines (ML) with broad-side coupling, structures with modal reservation (MR), reflection symmetric MLs, and modal filters (MF) with a passive conductor in the reference plane cutout and obtained the following results. It was found that the main reason for the additional pulses to appear in these structures is the introduction of asymmetry (of the cross-section, boundary conditions, and excitation). It is theoretically and experimentally established that additional pulses are a new resource for increasing the efficiency of protective devices with modal decomposition, but the highest effectiveness could be achieved through careful optimization.

Keywords: electromagnetic compatibility; intentional electromagnetic interference; ultrashort pulse; protection devices; modal filter; meander line; reflection symmetry; additional pulses; time response

1. Introduction

Radio-electronic equipment (REE) takes an increasingly significant place in human life. The use of electronics of varying level of complexity in various areas, from household to space, leads to aggravation of the electromagnetic compatibility (EMC) problem. The tendency to tighten EMC requirements arises because of the structural complication of REE, the increase in the upper frequencies of useful and interference signals and in the component density, as well as the need to take into account mutual influences at the levels of circuit elements, blocks, and systems.

Due to the improvements in the capabilities of intentional electromagnetic interference (IEMI) generators, protection against IEMI has been widely discussed in the EMC community in recent decades. So, for example, a special issue of the well-known journal «IEEE Transactions on Electromagnetic Compatibility» has been devoted to it, in which the IEMI threat to complex electronic systems that are important for human life is considered [1]. The susceptibility of various electronic devices to the threat of ultrawideband and high-power microwave pulses has been reviewed in [2], and the mechanisms of how disturbances penetrate into REE have been discussed in [3].

An important task of the EMC is to provide REE noise immunity. As is known, interfering signals are subdivided, depending on the propagation path, into radiated and conducted signals. Conducted interference is dangerous because it penetrates into REE directly through conductors—for example, through signal conductors or through power circuits [4]. To solve this problem,

protective devices (for example, LC- and RC-filters, varistors, arresters, TVS-diodes) connected to the protected circuit are traditionally used. However, there is conducted interference, the duration of which lies in the nanosecond and subnanosecond ranges. Such interference is called ultrashort pulses (USP) [5,6]. When a USP is formed, due to its short duration, the main energy of the generator is spent on increasing its amplitude [7]. The high amplitude of the interfering pulse leads to the breakdown of semiconductor devices [8] and capacitors in the noise-suppressing filters, and the response time of varistors and arresters can significantly exceed the duration of the USP [9], which makes them useless. In addition, under the USP influence on equipment, the energy does not have time to be distributed among the structural elements, and it localizes at one point, which increases the probability of failure in sensitive areas [10]. Particular attention should be given for the possibility of pulse trains to influence REE. For instance, the results of a novel laser configuration that can output 3.5 μm nanosecond laser pulses based on a simple and monolithic fiber structure are known [11].

The universally used protective devices may not be effective due to the USP features in the current electromagnetic environment; therefore, there is a need to develop new protective devices. In this regard, passive devices based on coupled transmission lines are noteworthy. For the analysis and optimization of such devices, quick analytical models for calculating the time response are convenient. So, for example, the paper [12] considers analytical models for calculating the amplitude of pulses at the output of a single segment of 2-, 3-, and 4-conductor transmission lines, and the paper [13] describes a multiconductor transmission lines simulation approach based on Pade approximations. Asymmetric coupled lines have also been considered. For instance, they have recently been investigated in relation to suppress common-mode noise in bent differential lines [14]. In the paper [15], the asymmetric coupled lines are considered and various systems of parameters, including per-unit length and modal ones, are presented. Moreover, in the paper [16], the authors propose analytical models for the time response suitable for structures of asymmetric coupled lines.

To protect REE from a USP, a modal filtration technology has been proposed, the principle of which is based on USP decomposition into a sequence of pulses of lower amplitudes [17]. This is feasible in strip structures with inhomogeneous dielectric filling, and the decomposition itself is feasible due to the difference in the delay of the modes propagating in these structures. Such devices are called modal filters (MF) and meander lines (ML) (or protective meanders). The condition for the complete pulse decomposition in an MF of length l is that the total pulse duration t_Σ be less than the minimum modulus of the difference in mode delays [17]:

$$t_\Sigma < l \min|\tau_i - \tau_k|,\ i, k = 1, \ldots, N,\ i \neq k \quad (1)$$

where $\tau_{i(k)}$ is the per-unit-length delay of the $i(k)$ line mode.

To improve the characteristics of such devices, it is advisable to optimize them according to various criteria. In addition, there is a possibility of changing the geometric configuration of such structures to create better conditions for the effective USP decomposition in an MF. It was found that keeping the symmetry of the structural cross-sections increases the efficiency of modal filtration [17]. For example, a research of the pulse propagation in a segment of a flexible printed cable with a symmetrical arrangement of conductors 1 m long relative to the reference conductor (ground) showed a 2-fold decrease of the exciting pulse amplitude with a duration of 0.3 ns. However, in the asymmetric structure, a significant decrease in the interference amplitude was not achieved. These results can be generalized to any segment of coupled lines (with the number of conductors $N = 2$), the cross-section of which is symmetrical about the axis passing through the reference conductor. Moreover, to obtain equal decomposition pulse amplitudes at the output of the structure at $N = 2$, the symmetry of the boundary conditions is important:

$$R = (Z_e Z_o)^{0.5} \quad (2)$$

where R is the value of the resistances at the ends of the line, and Z_e, Z_o are the impedances of the even and odd modes, respectively.

The most clearly demonstrated is the use of symmetry in order to improve modal filtration in MF structures with reflection symmetry. The most prominent representative of such structures is a reflection-symmetric MF [17]. Its cross-section with a reflection-symmetrical arrangement of conductors relative to the horizontal (α) and vertical (β) axes of symmetry is shown in Figure 1. The MF parameters are the following: w (the width of conductors), s (the separation of conductors), t (the thickness of conductors), h (the thickness of dielectric), d (the distance from the structure edge to the conductor), and ε_r (the relative permittivity of the dielectric).

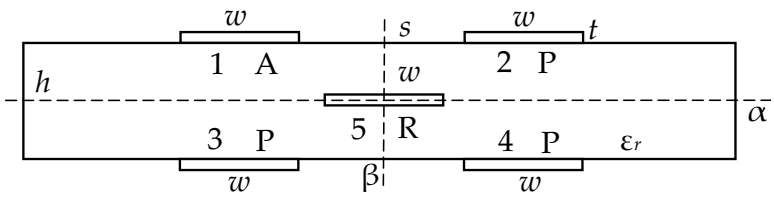

Figure 1. Cross-section of the reflection-symmetric modal filters (MF). Conductors: A—active, P—passive, R—reference.

Such a design provides both edge and broad-side couplings and makes it possible to obtain equal amplitudes of pulses and time intervals between them for certain geometric parameters (Figure 2). This fact is important because in problems of protecting REE from USPs, pairwise equalization of the output pulse amplitudes allows minimizing the maximum one, and close values of the time intervals between these pulses make it possible to increase the duration of the exciting USP (up to 450 ps, according to Figure 2, which will decompose completely). When simulating the time response to a pulse with an electromotive force (EMF) of 5 V and a total duration of 150 ps, it was found that the maximum value of the pulse amplitudes at the MF output was 0.625 V, which is 4 times less than the pulse amplitude at the MF input (2.5 V).

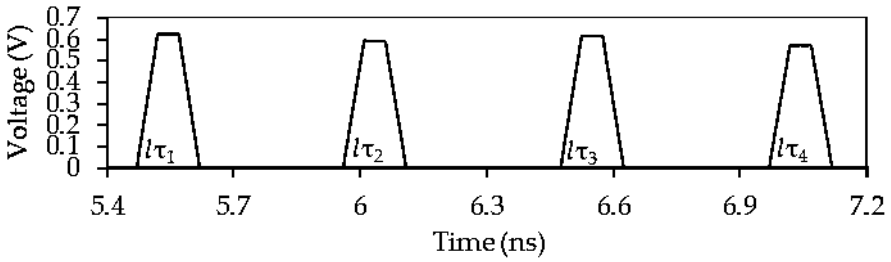

Figure 2. Voltage waveform at the output of the reflection-symmetric MF excited by a single pulse with an electromotive force (EMF) of 5 V.

Another approach to the USP modal decomposition into a sequence of lower amplitude pulses is based on its decomposition in an ML [18]. The choice of one ML turn parameters provides several conditions that contribute to the USP decomposition into 3 main pulses with smaller amplitudes, with the first pulse being crosstalk at the near line end and the second and third ones (the separated pulses of the even and odd modes). Note that in a similar structure of a two-conductor MF, only 2 pulses will be observed because of the lack of a crosstalk pulse at the near end of the line. It was shown that the USP can be decomposed into a sequence of 3 main pulses with the attenuation up to 6.3 times in one turn of the ML based on a microstrip structure and up to 4.6 times in one turn of the ML with broad-side coupling [18]. For example, Figure 3 shows the cross-sections of the ML based on the microstrip structure and with the broad-side coupling.

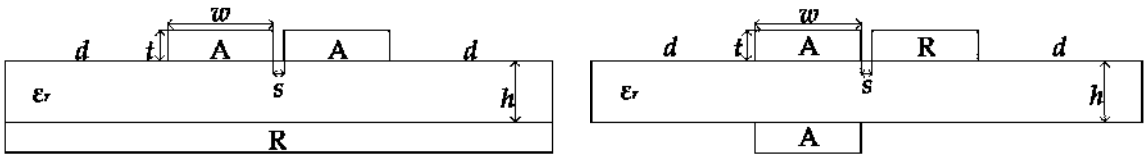

Figure 3. Meander lines (ML) cross-sections: (**a**) based on the microstrip structure and (**b**) with broad-side coupling.

One of the ways to develop modal filtration technology is modal reservation (MR), which is implemented based on cold standby. The main idea of MR is to trace reserved and reserving conductors on a printed circuit board (PCB) so that strong electromagnetic coupling is formed between them. As a result, it becomes possible to use modal distortions for the protection against USPs. The implementation of MR in a multilayer PCB is shown in Figure 4. The reserved circuit is positioned on PCB 1, and the reserving is positioned on PCB 2, with the reference conductor on the boards made in the form of separate layers. There is a dielectric layer between PCBs 1 and 2. The paths of the reserved and reserving circuits corresponding to each other are located in parallel and under each other in the dielectric medium; the components are located on the opposite sides of the PCBs. The attenuation of the USP has been considered before and after the failure of electronic components.

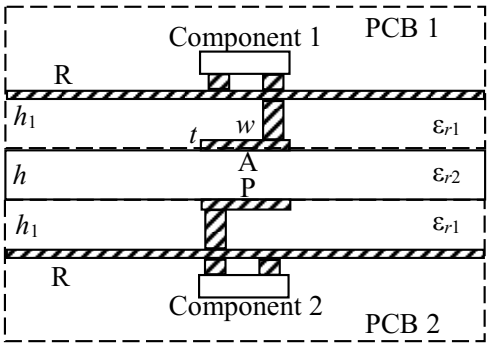

Figure 4. Multilayer printed circuit board (PCB) configuration for the circuit with MR. Conductors: A—active, P—passive, R—reference.

Remarkably, traditional strip MFs have a number of advantages—for example, good USP attenuation and small MF size. However, such MFs are not free from drawbacks: these include the complexity of implementation and the presence of a passive conductor, which takes up space and brings in additional mass. Therefore, it is important to explore new possibilities for MF realization. One of the simplest options for an MF is obtained by modifying a microstrip line (MSL). The design of such an MF is formed by means of two cutouts in the reference plane of a conventional MSL, which form a passive conductor between them (Figure 5). This solution is designed to simplify the implementation of the MF, as well as reduce its mass.

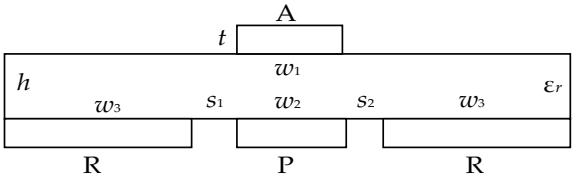

Figure 5. Cross-section of the MF with a passive conductor in the reference plane cutout. Conductors: A—active, P—passive, R—reference.

As noted earlier, to increase the efficiency of modal filtration, it is necessary to observe the axial symmetry of the structural cross-section. The symmetry of the boundary conditions for the case of coupled lines is also important [17]; it is expressed by the condition

$$R_1 = R_2 = R_3 = R_4, \tag{3}$$

for example, when the load values (R) at the ends of the line are taken equal to the value from (2) for the case of coupled lines, or the characteristic impedance of the path of 50 Ω for the case of multiconductor structures. Finally, the symmetry of the excitation is important when, in the structures with N = 3, 5, 7, ..., the excitation signal is fed to the central conductor. Thus, it is obvious that in all structures described above (the reflection-symmetric MF, the microstrip-based ML, the MR structures without failure, and the MF with a passive conductor in the reference plane cutout), the symmetry of the cross-section and boundary conditions is observed, and in some structures with MR: the symmetry of the excitation.

However, it is worth considering the MF in which the active and passive conductors are located asymmetrically with respect to the reference one (Figure 6a). The study of this structure without the use of resistors, in the case of a short circuit (SC) at the beginning of the passive conductor and an open circuit (OC) at the end (Figure 6b), has revealed some pulses with delays that are not multiples of even and odd mode delays. In addition, the authors have discovered the peculiarities of pulse shapes that differ from trapezoidal ones. To prove this statement, a quasistatic simulation has been performed under the excitation of the EMF of 5 V with rise, fall, and flat top times of 50 ps. Thanks to this, we were able to separate superimposed pulses and determine the pattern of their appearance. It was shown that their delays are described by linear combinations of the even and odd line mode delays. The voltage waveform at the output of such an MF is shown in Figure 7.

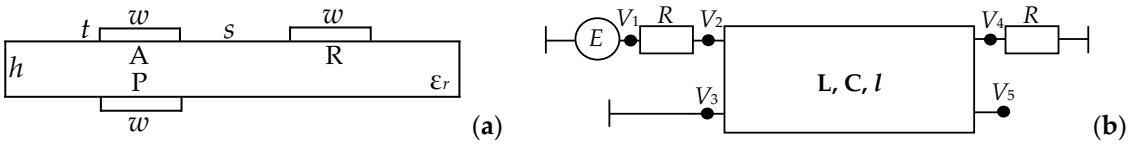

Figure 6. (**a**) Cross-section and (**b**) equivalent circuit of the asymmetric MF.

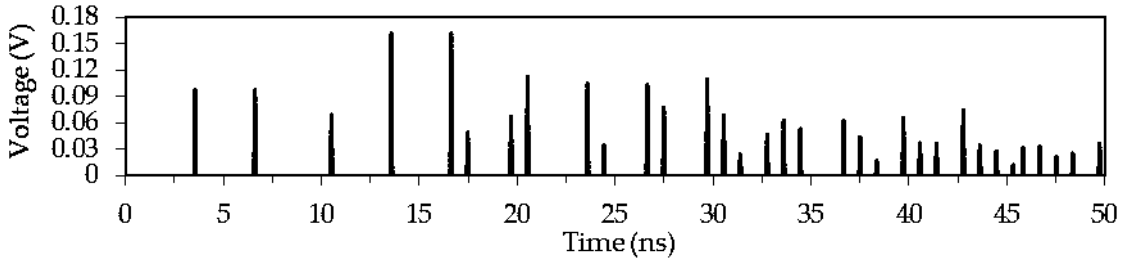

Figure 7. Voltage waveform at the asymmetric MF output.

These results are very important, since they imply the possibility of using additional pulses whose delays are not equal to or multiples of delays of the protective structure modes. This resource is hidden and not exploited. Meanwhile, it allows for an additional decrease in the maximum output voltage, as shown by a number of recent studies of the authors. It can be assumed that it is precisely symmetry that hides this resource, while asymmetry allows uncovering it.

It is important to note that the implementation of asymmetry into typical protection structures with modal filtration can improve their characteristics. This has been demonstrated in recent studies on the simulation of 2-, 3-, and 4-turn reflection symmetric MLs and the method for detecting additional pulses in these MLs. However, these particular results are published in publications covering a relatively narrow audience. Therefore, their rationalization and comprehension in a single extensive work is advisable.

In order to form a more complete picture of the role of symmetry and various types of asymmetry in the appearance of additional pulses, their parameter values, and the effect on modal decomposition, it is advisable to consider in a single paper the possibilities of their appearance in various structures. The purpose of this work is to carry out such research.

In spite of the fact that some cases of the additional pulse occurrences to be discussed below have recently been published by the authors (a reflection symmetric ML with the method for detecting additional pulses), a number of structures are presented here for the first time (a structure with double MR after failure, a turn of an ML with broad-side coupling, a structure with single MR after failure, an MF with a passive conductor in the cutout of the reference plane along with the experimental results). In addition, the systematization and analysis of such an extensive material on the example of various structures in a single work will help to formulate an improved method for detecting additional pulses. Finally, from the above review, it is clear that despite the fact that the idea of transmission line asymmetry has been mentioned earlier, its use as a hidden resource for improving the characteristics of protection devices is proposed by the authors in a single extensive work for the first time.

To achieve this aim, four types of protective structures were chosen as objects of the study: an ML, the structures with MR, an MF with a passive conductor in the reference plane cutout, and a reflection-symmetric MF. It was assumed that T-waves are propagating along the considered structures. Initially, cross-section geometric models of the structures under study were constructed. Then, based on these matrices **C** and **L** calculated as in [17], secondary characteristics were obtained: the matrixes of characteristic impedance ($\mathbf{Z}_C$) and per-unit-length mode delays (τ_i). If losses are important, the per-unit-length matrices of resistance **R** (conductors losses) and conductivities **G** (dielectrics losses) were calculated [17]. Finally, we drew a schematic diagram to simulate each structure, set loads, and EMF values, and we computed the time response to the excitation in the range of parameters. The signal parameters and waveforms were calculated in the TALGAT software [19], wherein the above-mentioned models and steps were implemented. To verify the quasistatic simulation results, we performed characteristics measurement and electrodynamic analysis for one of the structures and described them in the corresponding section.

2. Detection of Additional Pulses in Asymmetric Structures with Modal Filtration

2.1. Turn of the Meander Line with Broad-Side Coupling

First, let us consider the decomposition of a USP in an ML with broad-side coupling. Figure 3b shows the ML cross-section. The values of the parameters are the following: w = 15 mm; t = 105 μm; s = 1 mm; h = 6 mm; $d = w$; ε_r = 4. Figure 8a shows the circuit diagram of the turn. The line consists of two parallel conductors, each with the length of l = 1 m, interconnected at the far end. One of the conductors is connected to a pulse source in the near end, which is presented by the EMF source E and the internal resistance $R1$. Another conductor of the line is connected to a receiving unit, which is presented in the diagram as resistance $R2$. To minimize reflections, resistances $R1$ and $R2$ are taken equal to the geometric mean of the characteristic impedance of even and odd modes (including further simulation, when the structure parameters are changed). The calculated **C** and **L** matrices are:

$$\mathrm{C} = \begin{bmatrix} 137.89 & -96.94 \\ -96.94 & 122.44 \end{bmatrix} \mathrm{pF/m}, \mathbf{L} = \begin{bmatrix} 382.92 & 269.55 \\ 269.55 & 477.22 \end{bmatrix} \mathrm{nH/m}.$$

Then, we calculated the response to the USP with an EMF amplitude of 1 V and rise, flat top, and fall times of 1 ns. Figure 8b shows the voltage waveform at the turn output. As can be seen, the USP became a sequence of three main pulses of smaller amplitude up to 0.21 V. The first pulse is near-end crosstalk; the second and third ones are pulses of the even and odd modes of the line. However, there is a step with an amplitude of 0.114 V between the pulses of the even and odd modes of the line. There are also signal bursts on the fall and the front of the second and third pulses, respectively.

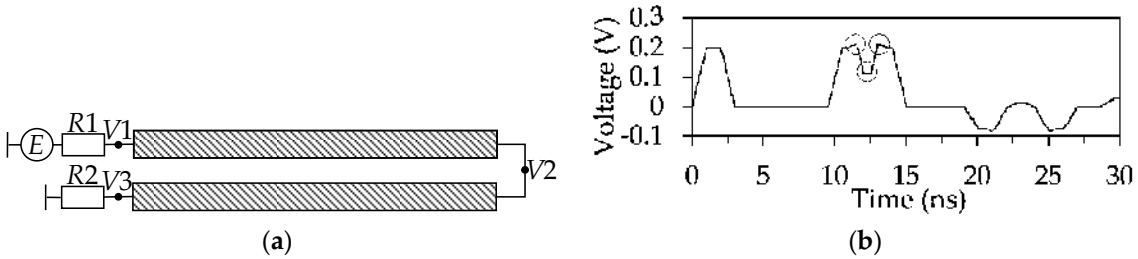

(**a**) (**b**)

Figure 8. (**a**) Circuit diagram and (**b**) output voltage waveform of ML with broad-side coupling.

In [18], the effect of changing the parameters of an ML with broad-side coupling on the USP attenuation has been examined. The optimal meander line parameters ensuring the fulfillment of the conditions were obtained

$$2\tau_e l \geq t_\Sigma, \quad (4)$$

$$2l|\tau_e\text{-}\tau_o| \geq t_\Sigma \quad (5)$$

where τ_e and τ_o are per-unit-length delays of even and odd line modes, respectively, and t_Σ is the total USP duration.

The fulfillment of condition (4) provides the arrival of the even mode pulse after the end of the crosstalk pulse, and (5) provides the decomposition of the main pulse into even and odd mode pulses. In addition, the optimization of the coupling between the signal conductors allows equalizing the amplitudes of these three pulses, and therefore minimizing the amplitude of the output signal. The optimal parameters of the ML with broad-side coupling are the following: w = 1 mm, t = 18 μm, s = 200 μm, h = 540 μm, d = 3 mm, ε_r = 5, l = 80 mm.

The calculated **C** and **L** matrices are:

$$\mathrm{C} = \begin{bmatrix} 128.89 & -93.5116 \\ -93.5116 & 120.31 \end{bmatrix} \mathrm{pF/m}, \mathbf{L} = \begin{bmatrix} 487.441 & 332.564 \\ 332.564 & 572.637 \end{bmatrix} \mathrm{nH/m}.$$

Per-unit-length delays of even and odd modes of the investigated structure were calculated: τ_e = 5.14 ns/m, τ_o = 6.56 ns/m. We considered in detail the waveform of the output signal (Figure 9a) in the line corresponding to the defined parameters and calculated the response to the USP with an EMF amplitude of 1 V and a flat top duration of 100 ps, as well as a rise time and fall time of 50 ps. As can be seen from the waveform in Figure 9a, the USP at the end of the line is decomposed into 3 main pulses. In this case, the maximum signal amplitude at the end of the line does not exceed 0.202 V. It is important to note that between the even and odd mode pulses we observed a step, which was similar to the one in Figure 8, but with smaller amplitude, not exceeding 12 mV; meanwhile, signal bursts are still observed at the fall of the second pulse and front of the third one. For clear demonstration of the presence of the pulse between the even and odd modes, we calculated the response when the line length increases. Figure 9b shows the calculated voltage waveform at l = 150 mm. It can be seen that the USP is presented by a sequence of 4 pulses: crosstalk ($P1$), even mode ($P2$), additional ($P3$), and odd mode ($P4$). Let us define the delays of each of them. Since pulse $P1$ is crosstalk, its arrival time is t_1 = 0 ns. The delay of pulse $P2$ (even mode pulse) is defined as $t_2 = 2l\tau_e$ = 1.54 ns and the delay of pulse $P4$ (odd mode pulse) is $t_4 = 2l\tau_o$ = 1.97 ns.

The delay of the additional pulse ($P3$) is defined as the arithmetic mean of the delays of the even and odd mode pulses and amounts $t_3 = (2l\tau_e + 2l\tau_o)/2 = l(\tau_e + \tau_o)$ = 1.75 ns. After determining the delays of each of the pulses, we can formulate the conditions for the complete decomposition of the USP into 4 pulses (crosstalk, even mode, additional, and odd mode). The first condition that provides the arrival of the even mode pulse after the end of the crosstalk pulse corresponds to condition (4). The second condition provides the arrival of the additional pulse at the end of the even mode pulse—$t_3 \geq t_2 + t_\Sigma$, and the third condition provides the arrival of the odd mode pulse at the end of the additional

pulse—$t_4 \geq t_3 + t_\Sigma$. After the substitution of the known variables and algebraic transformations, the second and third conditions will take the same form

$$l(\tau_o\text{-}\tau_e) \geq t_\Sigma. \quad (6)$$

After the substitution of the known values in (4) and (6), we obtain 1.54 ns ≥ 0.2 ns and 0.21 ns ≥ 0.2 ns, respectively. Thus, Figure 9b shows the case when conditions (4) and (6) are satisfied and the USP is decomposed into 4 pulses. For the case in Figure 9a, when we substitute the known values in (4) and (6), we obtain 0.82 ns ≤ 0.2 ns and 0.11 ns < 0.2 ns, respectively. Thus, conditions (4) and (6) are not satisfied, and the USP is decomposed only into 3 pulses.

The existence of the additional pulse gives an additional resource to USP amplitude attenuation. For this, it is necessary to equalize its amplitude with the amplitudes of other pulses, therewith to minimize the total amplitude at the end of the line. It seems possible to do this due to the parametric optimization of the structure.

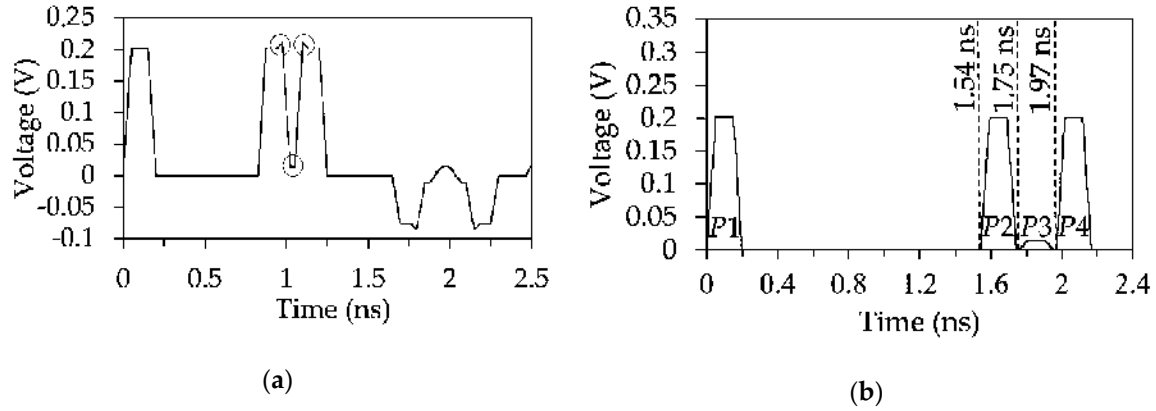

Figure 9. Voltage waveform at the end of ML with broad-side coupling for (**a**) l = 80 mm and (**b**) l = 150 mm.

Before the optimization, it is worth analyzing the effect of the cross-section parameters of the line on the amplitudes of each of the 4 pulses. The initial parameters are chosen so as to provide the fulfillment of conditions (4) and (6) and to exclude the superposition of pulses with a separate change of each parameter in a given range: w = 500 µm, t = 200 µm, s = 25 µm, h = 750 µm, d = 1500 µm, ε_r = 200, l = 80 mm. The range and step of the variable parameters are the following: 100, 200, . . . , 1000 µm for w, t and h; 5, 10, . . . , 50 µm for s; 25, 50, . . . , 300 for ε_r. Figure 10 shows the obtained dependences of the amplitudes of each of the 4 pulses on w, t, s, h and ε_r.

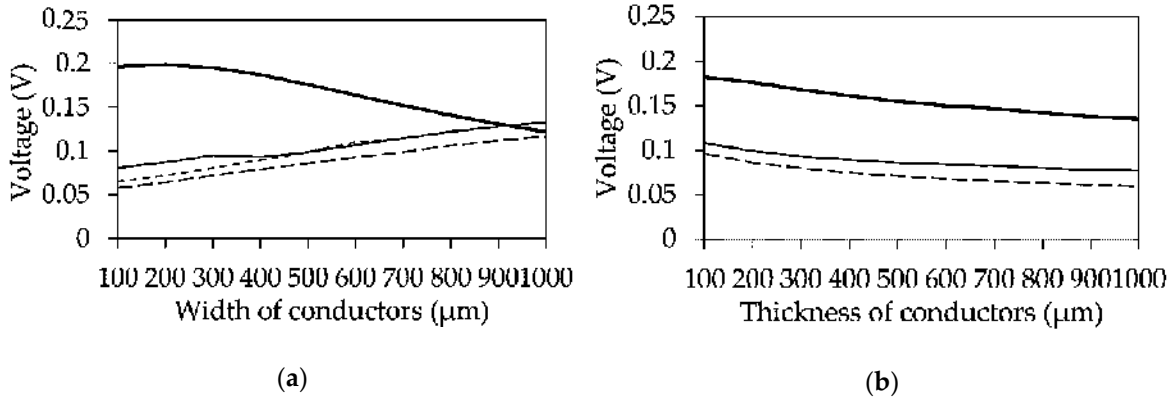

Figure 10. *Cont.*

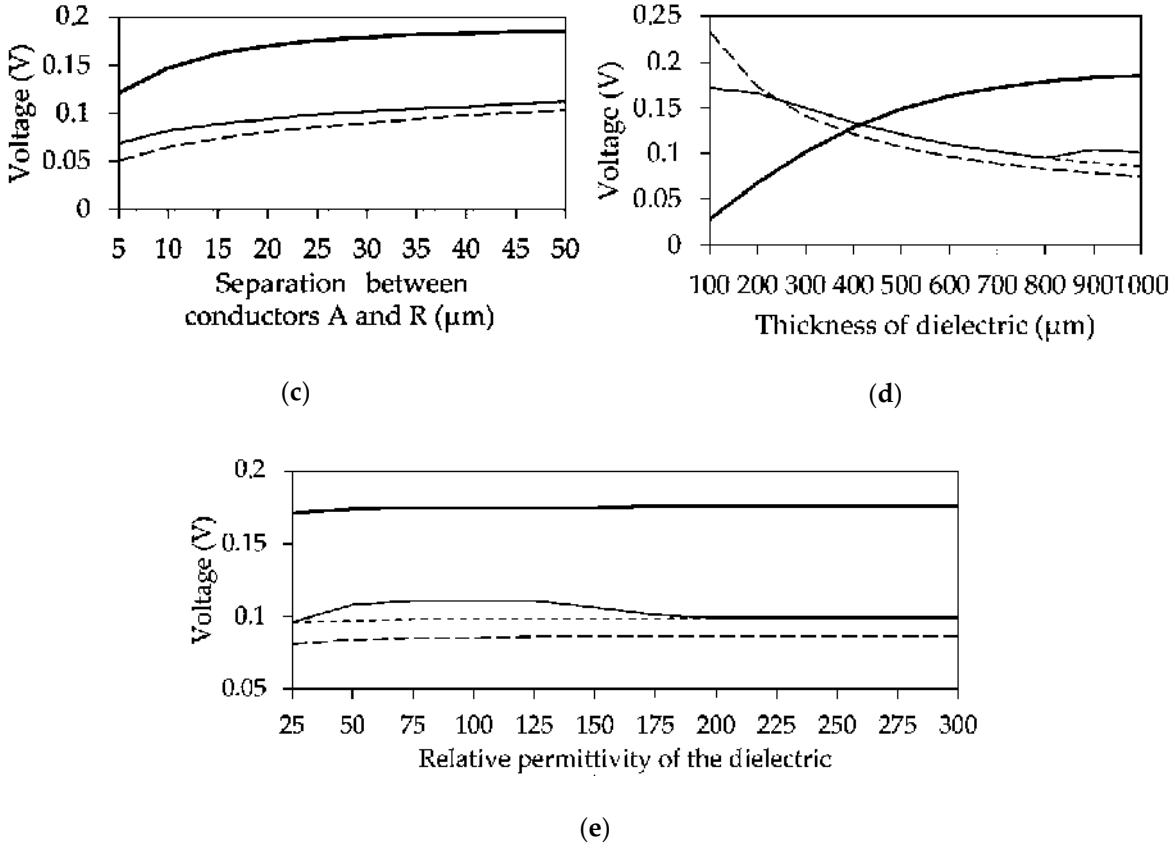

Figure 10. Dependencies of *P*1 (– –), *P*2 (- -), *P*3 (——), and *P*4 (——) pulse amplitude at the end of asymmetrical ML on w (**a**), t (**b**), s (**c**), h (**d**), and ε_r (**e**) with the original unchanged parameters.

As can be seen from Figure 10, when t increases, the amplitudes of all pulses monotonically decrease, and s increases. The increase of ε_r does not lead to a significant change in the amplitudes of the pulses. There is only a slight increase of the *P*4 pulse amplitude in the range of 25–200. From the t, s, and ε_r dependences, it can be seen that the amplitude of the output signal is determined by the pulse *P*3 amplitude. The dependences in Figure 10a,d are of interest, since the increase of w leads to the increase of the *P*1, *P*2, and *P*4 pulse amplitudes and the decrease of the *P*3 pulse amplitude; and the increase of h leads to the increase of the *P*3 pulse amplitude and the decrease of the *P*1, *P*2, and *P*4 pulse amplitudes. It is also seen that there are values of w and h for which the amplitudes of all pulses are almost the same; only the *P*1 pulse has a slight difference in amplitude. Thus, the minimization of the amplitude at the end of the line is more possible by equalizing the amplitudes of *P*2–*P*4 pulses. Based on this and taking into account conditions (4) and (6), using the heuristic search, we found the values of the optimal ML parameters from Figure 3b according to the criterion of minimizing the amplitude of the output voltage: w = 380 μm, t = 18 μm, s = 200 μm, h = 940 μm, $d = 3w$, ε_r = 20, and l = 150 mm. Figure 11a shows the output voltage waveform for these values of parameters. It can be seen from the waveform that the *P*2, *P*3, and *P*4 pulse amplitudes have the same value of about 0.151 V, which determines the maximum amplitude at the end of the line. The amplitude of pulse *P*1 is 0.127 V. The maximum attenuation is about 3 times.

A situation is possible when the pulses arrive at the end of the line with equal time intervals between pulses. The condition for such arrival for 3 pulses is

$$\tau_{max} = 2\tau_{min} \quad (7)$$

where τ_{min} and τ_{max} are the minimum and maximum of per-unit length delays of the even and odd modes, respectively. However, condition (7) does not take into account the additional pulse; therefore,

the time intervals between the 4 pulses in Figure 4 will not be equal. It is obvious that to take into account the additional pulse, condition (7) takes the form

$$\tau_{max} = 3\tau_{min}. \quad (8)$$

Consider the case when condition (8) is fulfilled. For this, we made an optimal parameter search and obtained: w = 1000 μm, t = 136 μm, s = 5 μm, h = 1200 μm, d = 3000 μm, ε_r = 500, and l = 80 mm. The calculated per-unit length delays were τ_e = 19.6 ns/m, and τ_o = 58.6 ns/m. Figure 11b shows the voltage waveform under condition (8). It can be seen that the USP at the end of the line became a sequence of pulses with equal time intervals between them. After the arrival of the first 4 pulses, the pulses caused by reflections arrived. The amplitude at the end of the line was 0.146 V. It is noteworthy that in this example, it is determined specifically by an additional pulse.

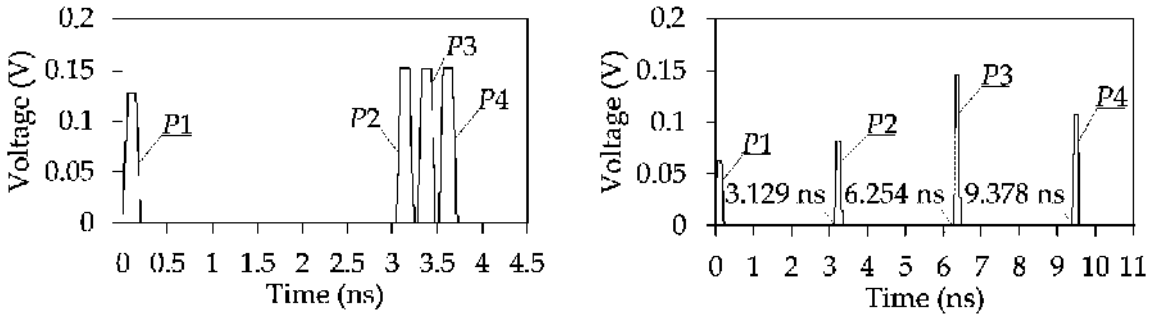

Figure 11. Voltage waveform at the ML output (**a**) with optimal parameters and (**b**) under condition (8).

Thus, it was demonstrated that the existence of an additional pulse is a resource for minimizing the output signal amplitude. The conditions providing the arrival of each decomposed pulse after the fall of the previous pulse were formulated. The cross-section parameters of the line were shown to have an influence on the amplitudes of the main decomposition pulses. It was revealed that the change of the signal conductor width and the dielectric thickness has the greatest influence; and the signal amplitude minimum at the end of the line is determined by the amplitude of the additional pulse and the even and odd mode pulses of the line. On the simulation example, it was shown that thanks to the additional pulse, it is possible to increase the USP attenuation in the line. The maximum attenuation of the USP amplitude up to 3 times was obtained. Finally, we formulated the condition that provides the arrival of each of the 4 pulses to the line end with equal time intervals between the neighboring pulses. It is obvious that by optimizing the ML according to the required criteria, it is possible to improve the protection against a USP with the help of the ML, which is asymmetric in the cross-section.

2.2. Additional Pulses in the Structure with Modal Reservation

2.2.1. Additional Pulses in the Structure with Modal Reservation after Failure

We studied a fabricated PCB prototype with MR in the 50 Ω path (Figure 12a). It includes sets of electrical connections with a single MR. The PCB stack is shown in Figure 12. For the Rogers RO3010 insulator, it was assumed that ε_{r2} = 10.2; for the FR-4 prepreg, ε_{r1} = 4.

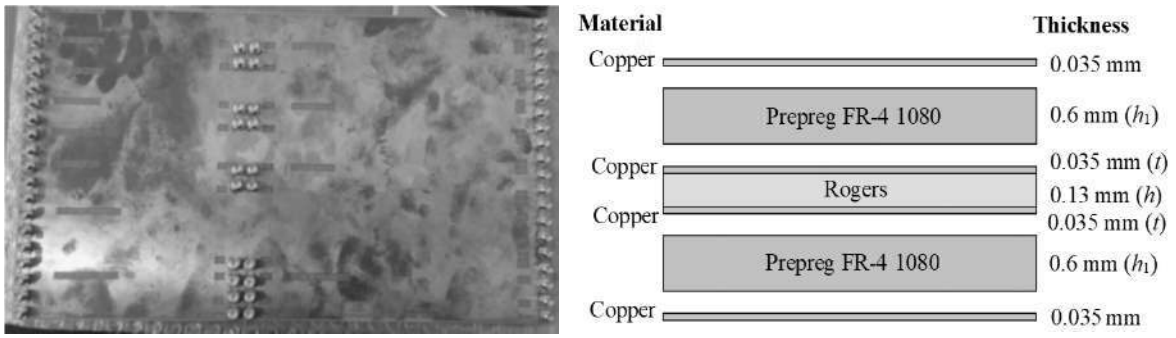

(**a**) (**b**)

Figure 12. (**a**) Photograph of the PCB prototype with modal reservation (MR); (**b**) PCB stack.

The PCB cross-section is presented in Figure 13a, with the values used from Figure 12b. The parameter values were the following: w = 185 µm, d = 555 µm, the distance from the end of the conductor to the side wall, d_1 = 740 µm.

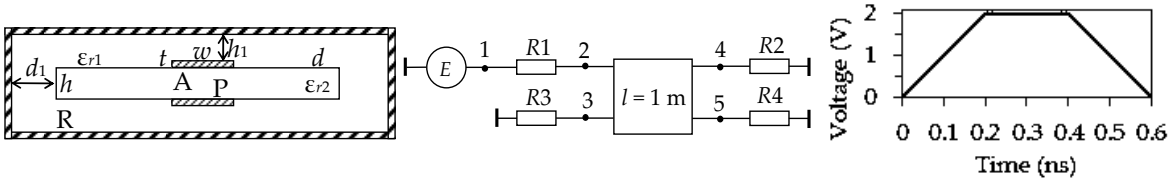

(**a**) (**b**) (c)

Figure 13. (**a**) Cross-section; (**b**) equivalent circuit of a structure with a single MR; (**c**) EMF waveform.

An equivalent circuit for simulating a 1-m long structure is shown in Figure 4b. In case of failure, it is assumed that the reserving circuit takes over the functions of the reserved one. The values of the resistors $R1$ and $R2$ were chosen to be equal to 50 Ω, while for $R3$ and $R4$: 50 Ω; 1 MΩ (to simulate an OC); 1 µΩ (to simulate an SC).

We obtained mode per-unit length delays for the PCB in Figure 13a (7.34 and 9.52 ns). Figure 13c shows the EMF waveform with an amplitude of 2 V and with a total duration of 600 ps. Figures 14 and 15 show the voltage waveforms at node 2 (Figure 13b) and node 4 (Figure 13b). In Table 1, the peak values of the main and additional pulses are summarized, which can be expressed in terms of τ_1 and τ_2. In working condition, when resistors at the ends of the passive conductor are 50 Ω, and the EMF is 1 V, at the far end, there are two decomposition pulses of 0.425 V. The amplitudes of the reflected pulses with delays of $2l\tau_1$ and $2l\tau_2$, $4l\tau_1$, and $4l\tau_2$ at the near end and $3l\tau_1$ and $3l\tau_2$, $5l\tau_1$, and $5l\tau_2$ at the far end decrease; however, no additional pulses are observed. In case of an SC or OC at one end of the passive conductor, the voltage waveforms at nodes 2 and 4 change. This is due to the change in the boundary conditions of the passive conductors and its influence on the mode matching. At the near end of the active conductor with an SC or OC on the passive conductor, the responses are different. At the far end of the active conductor for an OC, the first pulse is larger in amplitude by 0.16 V, and the second is 0.16 V smaller than in the working state (±38%), with the maximum amplitude of the pulses being 0.58 V. For an SC, on the contrary, the first pulse is 0.16 V less, and the second is 0.16 V higher than in the working state. The delay times of the reflected pulses are different, and for an SC or OC, they have different polarity.

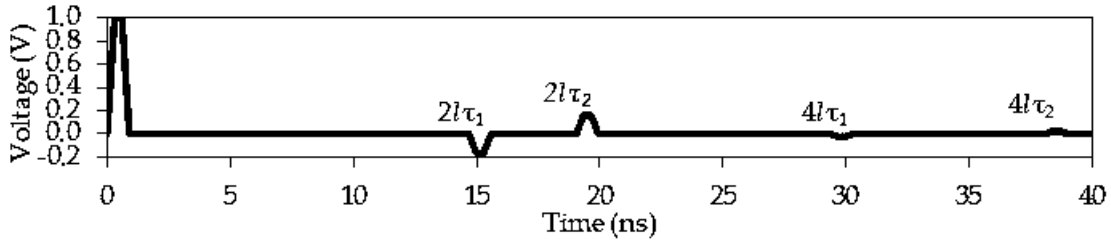

(**a**)

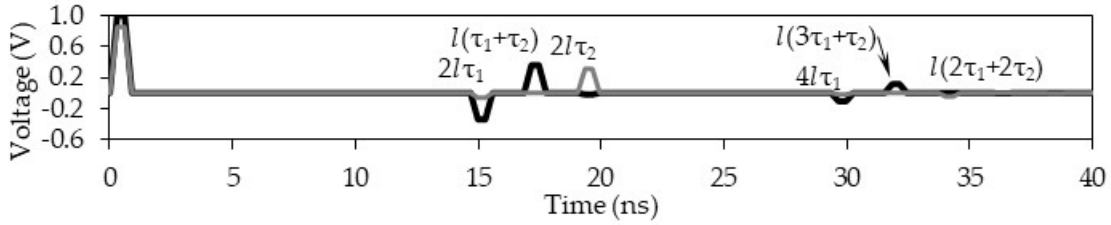

(**b**)

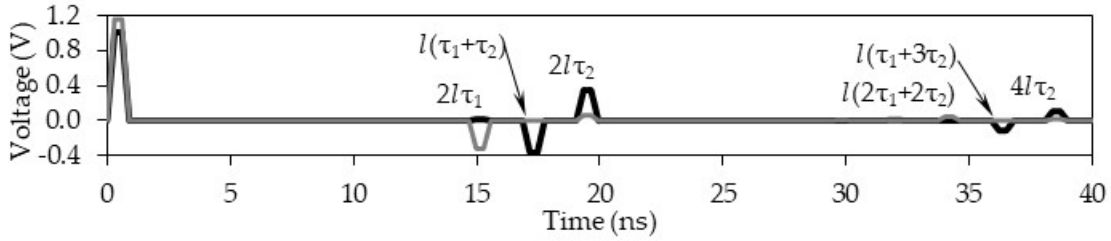

(**c**)

Figure 14. Voltage waveforms at the near end of the active conductor in the structure with a single MR for (**a**) 50 Ω, (**b**) short circuit (SC), (**c**) open circuit (OC) at the near (-) or far (=) end of the passive conductor.

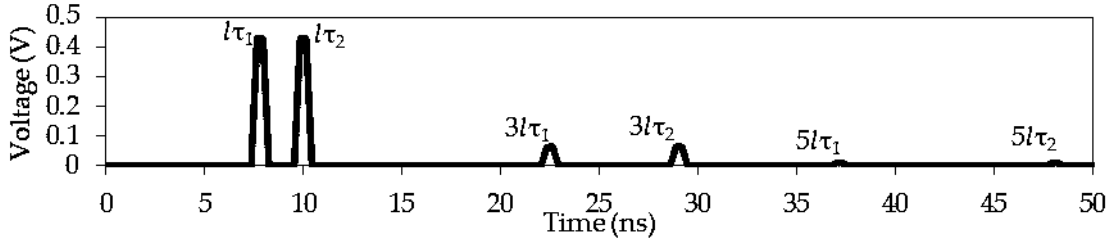

(**a**)

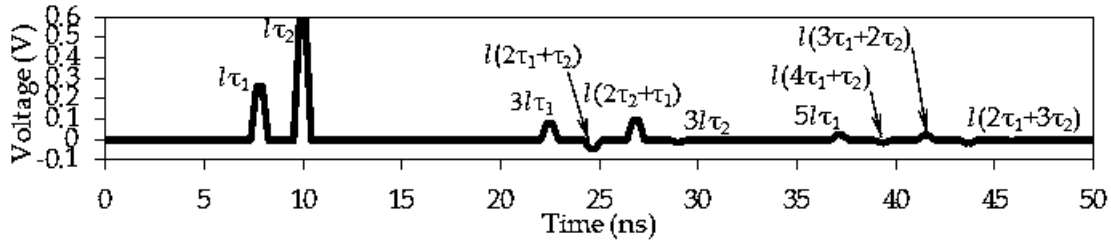

(**b**)

Figure 15. *Cont.*

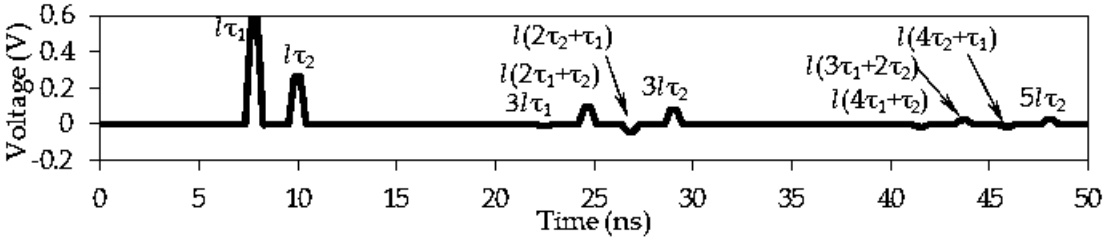

(**c**)

Figure 15. Voltage waveforms at the far end of the active conductor in the structure with a single MR for (**a**) 50 Ω, (**b**) SC, (**c**) OC at one end of the passive conductor.

Table 1. Delays of the main and additional pulses at the near and far ends of the active conductor with SC and OC at the near/far end of the passive conductor.

	***t*, ns**	***U*, V**		
		50 Ω	**SC**	**OC**
$l\tau_1$	7.34	0.425	0.262	0.589
$l\tau_2$	9.52	0.425	0.59	0.262
$2l\tau_1$	14.68	–0.165	–0.062/–0.344	–0.317/0.015
$l(\tau_1 + \tau_2)$	16.86	0	0/0.361	0/–0.364
$2l\tau_2$	19.04	0.162	0.311/–0.19	0.061/0.346
$3l\tau_1$	22.02	0.063	0.0818	–0.009
$l(2\tau_1 + \tau_2)$	24.2	0	–0.043	0.097
$l(2\tau_2 + \tau_1)$	26.38	0	0.097	–0.043
$3l\tau_2$	28.56	0.063	–0.009	0.082
$4l\tau_1$	29.36	–0.025	–0.019/–0.108	0.004/0
$l(3\tau_1 + \tau_2)$	31.54	0	0/0.114	0/0.005
$2l(\tau_1 + \tau_2)$	33.72	0	–0.045/0	0.045/0
$l(\tau_1 + 3\tau_2)$	35.9	0	0/–0.006	0/–0.112
$4l\tau_2$	38.08	0.023	–0.005/0	0.018/0.106
$5l\tau_1$	36.7	0.009	0.026	0
$l(4\tau_1 + \tau_2)$	38.88	0	–0.013	–0.002
$l(3\tau_1 + 2\tau_2)$	41.06	0	0.023	–0.015
$l(2\tau_1 + 3\tau_2)$	43.24	0	–0.015	0.023
$l(\tau_1 + 4\tau_2)$	45.42	0	–0.002	–0.013
$5l\tau_2$	47.6	0.009	0	0.026

Figure 16 shows the voltage amplitudes of the main and additional pulses with an increase in $R3$ or $R4$ from 0 to 1000 Ω (with a further increase in R, the voltage does not change). The main pulses with delays $l\tau_1$ and $l\tau_2$ vary in the range from 0.262 to 0.589 V, the reflected pulses with delays $3l\tau_1$ and $3l\tau_2$ vary in the range from 0.009 to 0.082 V, and with $5l\tau_1$ and $5l\tau_2$ vary in the range from 0 to 0.025 V. Additional pulses are also in these ranges, but unlike the main ones, which change smoothly, they change in another manner. Interestingly, with each new reflection, the number of additional pulses increases by two. Additional pulses between pulses with delays $7l\tau_1$ and $7l\tau_2$ are also observed, but their amplitudes are insignificant; therefore, they are not considered here.

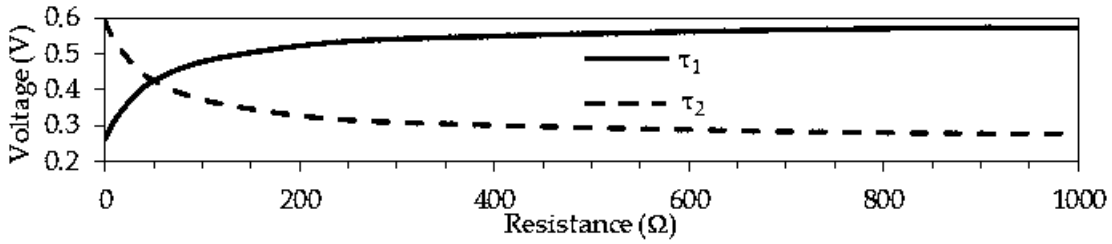

(**a**)

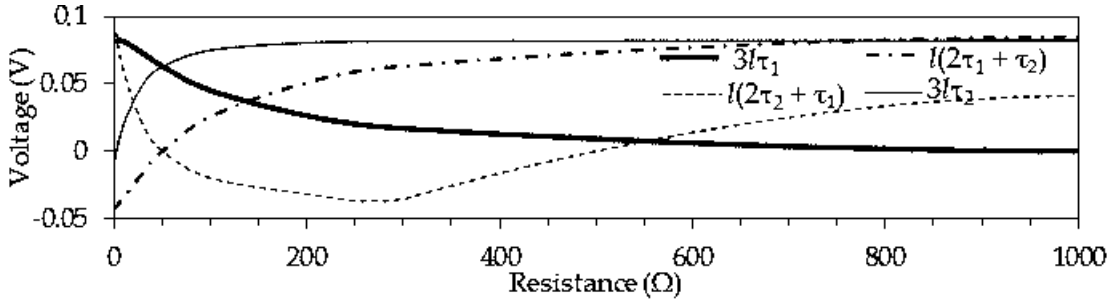

(**b**)

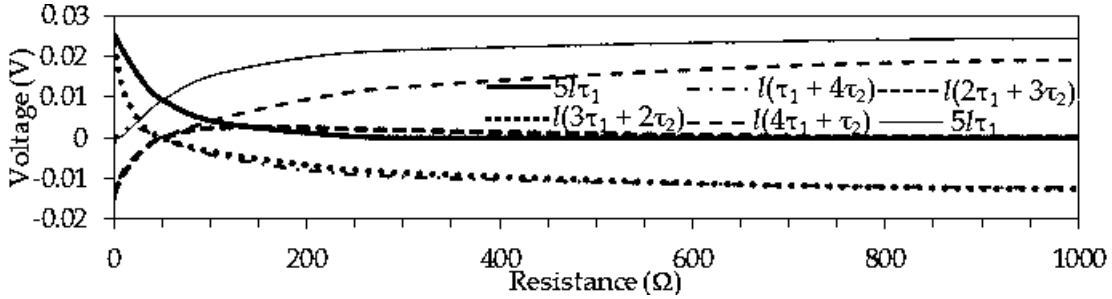

(**c**)

Figure 16. Voltage amplitudes of each of the pulses at the far end of the active conductor between the delays (**a**) $l\tau_1$ and $l\tau_2$, (**b**) $3l\tau_1$, $3l\tau_2$, $l(2\tau_1 + \tau_2)$ and $l(2\tau_2 + \tau_1)$, (**c**) $5l\tau_1$, $5l\tau_2$, $l(3\tau_1 + 2\tau_2)$, $l(\tau_1 + 4\tau_2)$, $l(4\tau_1 + \tau_2)$, and $l(2\tau_1 + 3\tau_2)$.

Thus, we considered the failure of the system components with MR in the 50 Ω path. Theoretically, the circuit was in working condition if all of the resistors were 50 Ω, and if one component of the system failed, an SC or OC was formed at a certain end of the circuit. The appearance of additional pulses is shown both at the near and at the far ends of the active conductor when the boundary conditions change from 50 Ω at one end of the passive conductor. It is also noteworthy that the polarity changes and the amplitudes of some pairs of additional pulses are equal when passing through the point R = 50 Ω. Meanwhile, the maximum signal amplitude, in this case, is determined not by additional, but by the main mode pulses.

2.2.2. Structure with Double Modal Reservation after Failure

The structure with double MR was studied using the example of simulating a three-wire structure with an additional dielectric. The cross-section of the structure is shown in Figure 17. Simulation parameters were w = 185 μm, t = 36 μm, d = 555 μm, s = 85 μm, h = 200 μm, ε_{r1} = 4, and ε_{r2} = 30.

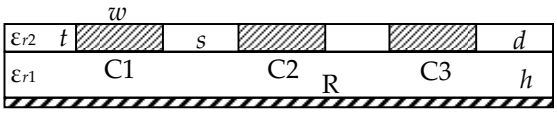

Figure 17. Cross-section of the three-conductor microstrip structure with an additional dielectric.

Equivalent circuits for simulating a three-conductor structure with a length of 1 m and with double MR are presented in Figure 18. In the simulation, for Figure 18a,b, the values of the active conductor resistors *R*1 and *R*2, as well as *R*3 and *R*4, respectively, were chosen equal to 50 Ω. The resistors for the passive conductors were set to 50 Ω, 1 MΩ (OC), and 1 μΩ (SC) for different failure modes.

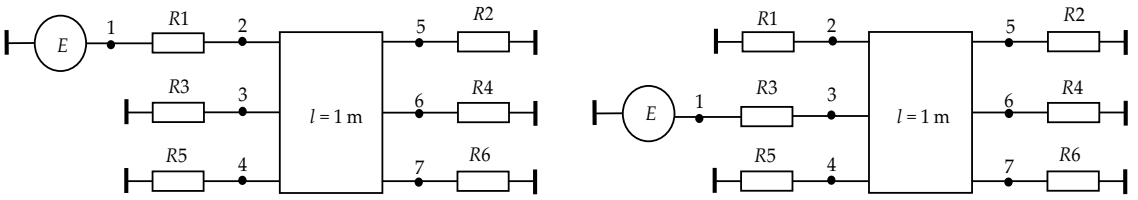

Figure 18. Equivalent circuits of the three-conductor structure for (**a**) extreme and (**b**) average active conductors.

At the input of the structure under study (Figure 18), a USP with an EMF of 2 V and the front, flat top, and fall times of 200 ps is applied. For the circuit in working condition (the resistor values of all passive conductors correspond to 50 Ω), Figure 19a shows the voltage waveforms at the near end of a three-wire structure with the side (node 2 in Figure 18a) and middle (node 3 in Figure 18b) active conductors. Figure 19b shows the voltage waveforms at the far end of a three-wire structure with the side (node 5 in Figure 18a) and middle (node 6 in Figure 18b) active conductors, and it also shows the amplitudes of 0.499 and 0.581 V, respectively. The pulse delays in response are 6.85, 7.7, and 8.8 ns. As can be seen, in a symmetric case (the middle conductor), there is not a second pulse. This doubles the duration of the pulse, which will decompose completely. However, an asymmetric excitation (the side conductor) gives a slightly lower amplitude of the output voltage.

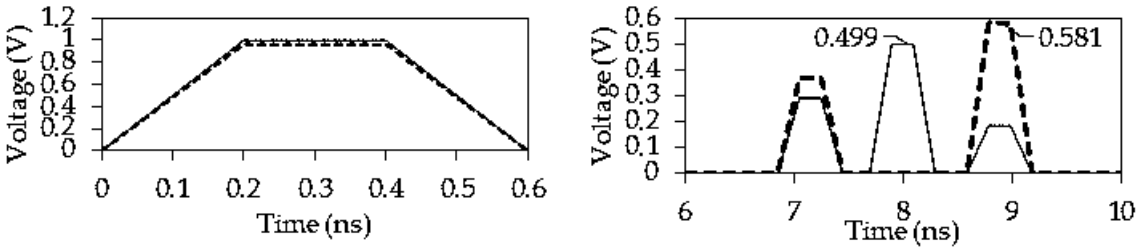

Figure 19. Voltage waveforms at the (**a**) near and far (**b**) ends of the three-conductor structure with side (-) and middle (- -) active conductors.

Figures 20 and 21 show the voltage waveforms at the far end of the three-conductor structure with the side and middle active conductors in the structure with MR under various boundary conditions. For an OC (Figure 20) at the far ends of the passive conductors, the maximum voltage amplitudes of the pulses at the far end of the active conductor are less than in the working state. For an SC (Figure 21) at the far ends of the passive conductors, the maximum pulse voltage amplitudes at the far end of the active conductor are either equal to or greater than in the operating state.

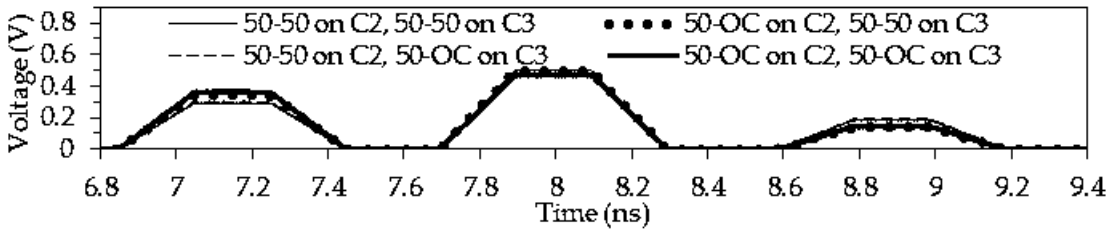

(**a**)

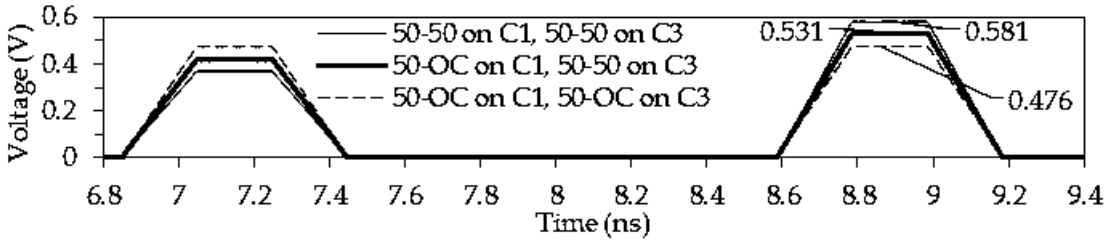

(b)

Figure 20. Voltage waveforms at the far end of the active conductor in the structure with MR for an OC at one end of the passive conductor with active conductors (**a**) C1, (**b**) C2.

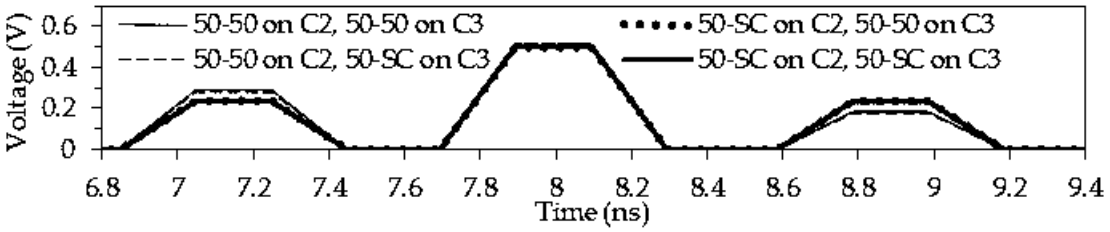

(**a**)

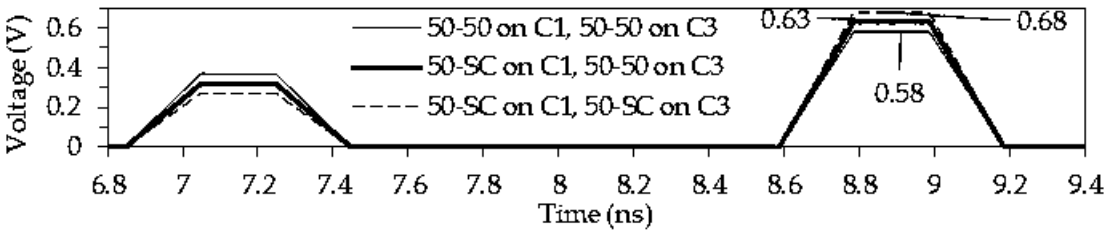

(**b**)

Figure 21. Voltage waveforms at the far end of the active conductor in the structure with an MR for an SC at one end of the passive conductor with active conductors (**a**) C1, (**b**) C2.

Thus, we considered the failure of the system components with MR. Theoretically, the circuit was in working condition if all of the resistors were 50 Ω, and if one component of the system failed, an SC or OC was formed at a certain end of the circuit. In the working state, the difference in the pulse delays at the far end of the active conductor is approximately twice as large as with the side active conductor, but the maximum amplitude is 16% larger. In the case of an SC at one end of the side or both conductors, the maximum amplitude at the far end of the active conductor P2 increases by 8.8% and 16.9%, respectively. In other cases, the maximum amplitude either stays unchanged or decreases.

Thus, in case of failures, the change in signal amplitude is small. Meanwhile, a detailed analysis of the results allows us to formulate the most preferable choice and order of circuit switching for MR.

As a result, symmetric excitation of the structure with double MR allows us to decompose the excitation pulse into 2 pulses with a maximum amplitude of 0.581 V, while under asymmetric excitation, we have 3 pulses with a maximum amplitude of 0.499 V, which is lower by 14%. In case of an SC, on one of the passive conductors, maintaining symmetric excitation, the maximum amplitude is 0.68 V, while under asymmetric excitation, the maximum amplitude is 0.499 V, which is lower by 31%.

2.3. Research of Reflection Symmetric Meander Lines

To acquire a more complete understanding of additional pulses, it is advisable to consider the possibility of their appearance in a structure where the axial symmetry of the cross-section and the symmetry of the boundary conditions are used simultaneously. From the results presented above, it becomes clear that the probability of their appearance in such structures is small, since they are hidden due to the symmetry. In this section, we present the simulation results of the structures obtained from a reflection symmetric MF (Figure 22) by means of various options for the electrical connection of conductors at the ends of the line using bridges instead of resistive terminations to the ground, so that the resulting structure is a reflection symmetric ML. With such a connection of half-turns, the symmetry of the boundary conditions is broken.

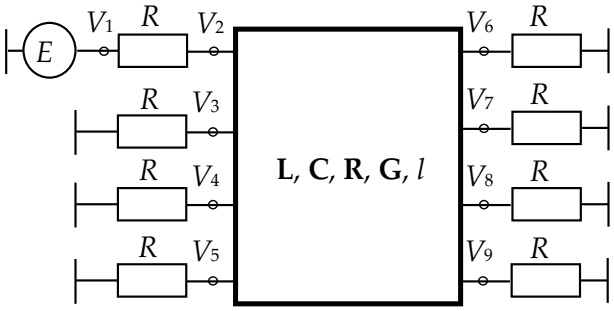

Figure 22. Equivalent circuit of a reflection symmetric MF.

2.3.1. Reflection Symmetric Meander line of 2 Cascaded Half-Turns

This subsection considers the reflection symmetric ML configuration, in which the signal travels a distance 2l (in 2 cascaded half-turns), with the 2 remaining conductors having resistors connected at their ends. In this case, 3 options for connecting half-turns are possible. Figure 23 presents the circuits, in which half-turns are paired conductors connected on top (conductors 1 and 2), on the side (conductors 1 and 3), and diagonally (conductors 1 and 4) (see Figure 1).

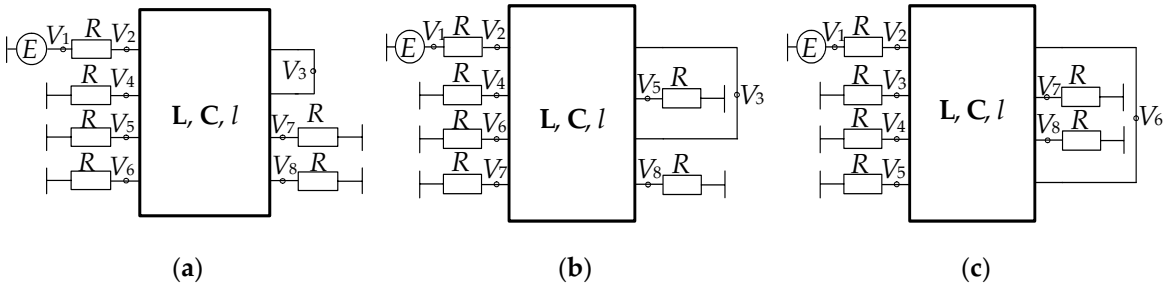

Figure 23. Equivalent circuits of 2 half-turn reflection symmetric ML: (**a**) 1, (**b**) 2 and (**c**) 3.

Simulation was performed with optimal cross-sectional parameters obtained previously for the reflection symmetric MF (s = 0.51 mm, w = 1.6 mm, t = 0.018 mm, h = 0.5 mm, ε_r = 4.5). Figure 24 presents the simulation results of the time response to a trapezoid pulse with an EMF amplitude of 5 V

with rise, flat top, and fall times of 50 ps (voltage waveforms are obtained at nodes V_4 in Figure 23a, V_6 in Figure 23b, and V_5 in Figure 23c).

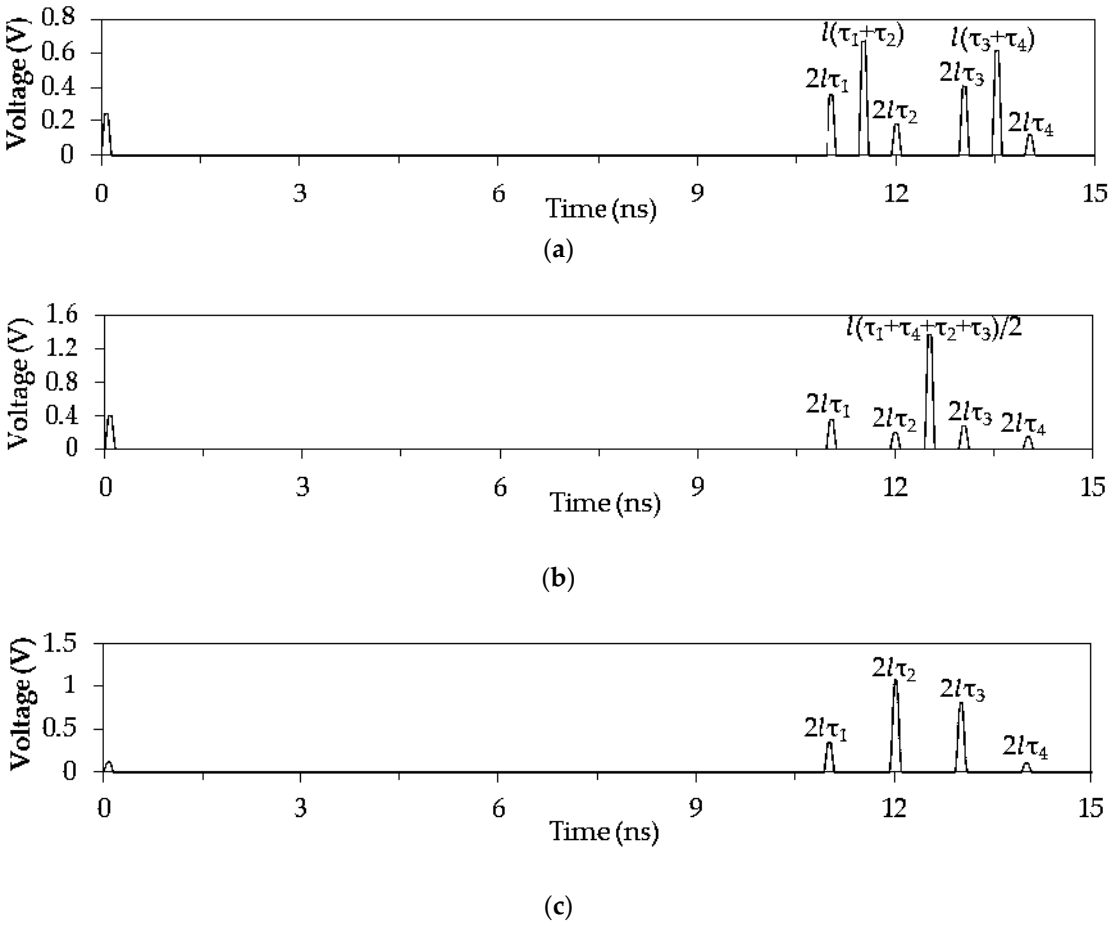

Figure 24. Voltage waveforms at the output of the 2 half-turn circuits with l = 1 m: (**a**) 1, (**b**) 2 and (**c**) 3.

On the obtained voltage waveforms, there are pulses whose delays are equal to the double delays of the 4 modes. However, it can be assumed that there are more additional pulses, but they arrive almost simultaneously with the main ones as a result of partial symmetry. For circuit 2, this can be confirmed by the fact that the pulse amplitude between pulses of modes 2 and 3 increases, and for circuit 3, the amplitude of the modes 2 and 3 pulses themselves increases. To confirm this hypothesis, the value of l is increased from an initial 1 m to 8 m for circuits 2 and 3. Figure 25 shows fragments of time responses (from 86 ns to 113 ns) for this case.

The results of the simulation confirm the hypothesis regarding the presence of additional pulses in circuit 3. However, for circuit 2, it was not possible to achieve decomposition of the pulse between modes 2 and 3 by increasing the length of the ML because in the reflection symmetric MF, which was taken as a prototype, the time intervals between decomposition pulses are equal. We will try to change the cross-sectional parameters of the structure for circuit 2 (i.e., introduce asymmetry by reducing the broad-side coupling between the conductors): s = 0.51 mm, w = 1.6 mm, t = 0.018 mm, ε_r = 4.5 are unchanged, and the h value is increased from 0.5 to 1 mm. The output voltage waveforms of circuit 2 are shown in the Figure 26 where 2 additional pulses appeared.

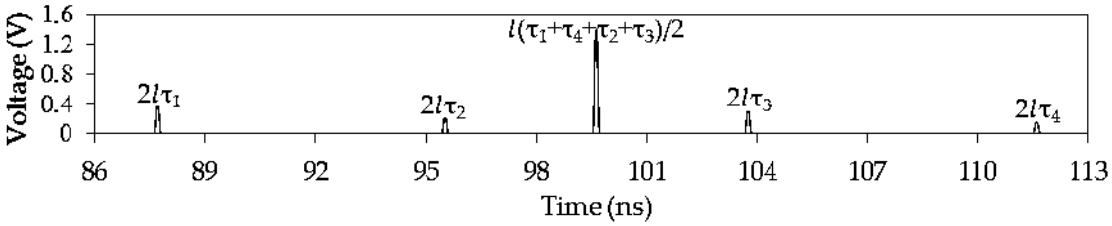

(**a**)

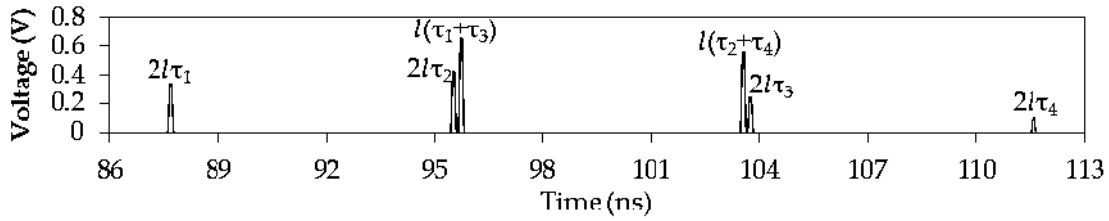

(**b**)

Figure 25. Voltage waveforms at the output of the 2 half-turn circuits with l = 8 m: (**a**) 2, (**b**) 3.

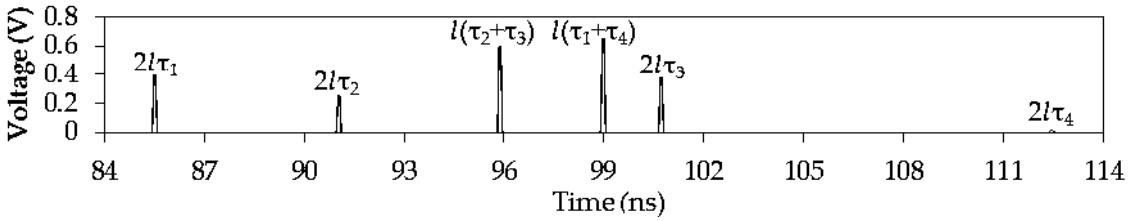

Figure 26. Voltage waveforms at the output of circuit 2 with l = 8 m and h = 1 mm.

For convenience, Table 2 summarizes the values of per-unit length delays of the main pulse (modes 1–4). Table 2 also has values of per-unit length delays that are multiplied by 2 and 16 because the delays of main pulses at the output of the reflection symmetric ML are multiples of 2 and 16 per-unit length delays for l = 1 m and l = 8 m, respectively.

Table 2. Per-unit length delays (ns/m) for modes 1–4, multiplied by 1, 2, 4, and 16.

Multiplier	1	2	3	4
1	5.4698	5.9591	6.4746	6.9687
2	10.9398	11.9183	12.9493	13.9376
16	87.5168	98.3456	103.5936	111.4992
16 (h = 1 mm)	85.4332	90.9643	100.6443	112.3761

The analysis of the data in Table 2 and the time responses in Figures 24–26 show that the additional pulse delays are equal to the arithmetic mean of the delays that are multiples of double delays or simply the sum of 2 mode delays in different versions. Thus, for circuit 1, these delays are equal $l(2\tau_1 + 2\tau_2)/2 = l(\tau_1 + \tau_2) = 11.4289$ ns and $l(2\tau_3 + 2\tau_4)/2 = l(\tau_3 + \tau_4) = 13.4433$ ns, for circuit 2, these delays are $l(2\tau_1 + 2\tau_4)/2 = l(\tau_1 + \tau_4) = 12.4385$ ns and $l(2\tau_2 + 2\tau_3)/2 = l(\tau_2 + \tau_3) = 12.4337$ ns, and for circuit 3, these delays are $l(2\tau_1 + 2\tau_3)/2 = l(\tau_1 + \tau_3) = 11.9444$ ns and $l(2\tau_2 + 2\tau_4)/2 = l(\tau_2 + \tau_4) = 12.9278$ ns. However, due to the symmetry, coincidences are observed in the values of the additional pulse delays: in circuit 2, they coincided with each other, and in circuit 3, they coincided with the main pulses. As for the attenuation in the cases considered, the smallest output amplitude of all the circuits under consideration is equal to 0.661 V (at the output of circuit 1). Meanwhile, it almost matches the

value of the maximum amplitude of the reflection symmetric MF, which is 0.625 V. It is noteworthy that only 4 instead of 6 resistors are required at the ends of the passive conductors.

2.3.2. Reflection Symmetric Meander Line of 3 Cascaded Half-Turns

We consider the reflection symmetric ML in which the signal travels a distance 3*l* (in 3 cascaded half-turns). At the same time, resistors are connected at the ends of the fourth conductor. The three circuits obtained give various output voltage waveforms (Figure 27).

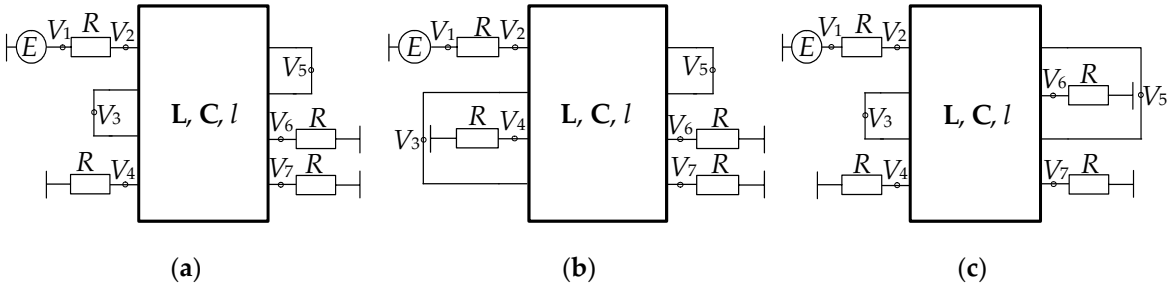

Figure 27. Equivalent circuits of 3 half-turns reflection symmetric ML: (**a**) 1, (**b**) 2 and (**c**) 3.

Optimal values of parameters (s = 0.51 mm, w = 1.6 mm, t = 0.018 mm, h = 0.5 mm, ε_r = 4.5) were selected to construct the geometric cross-section model. The time responses of the structures under investigation for l = 1 m were calculated similarly to Section 2.3.1. These are shown in Figure 28 (nodes V_6 in Figure 27a, c and V_7 in Figure 27b).

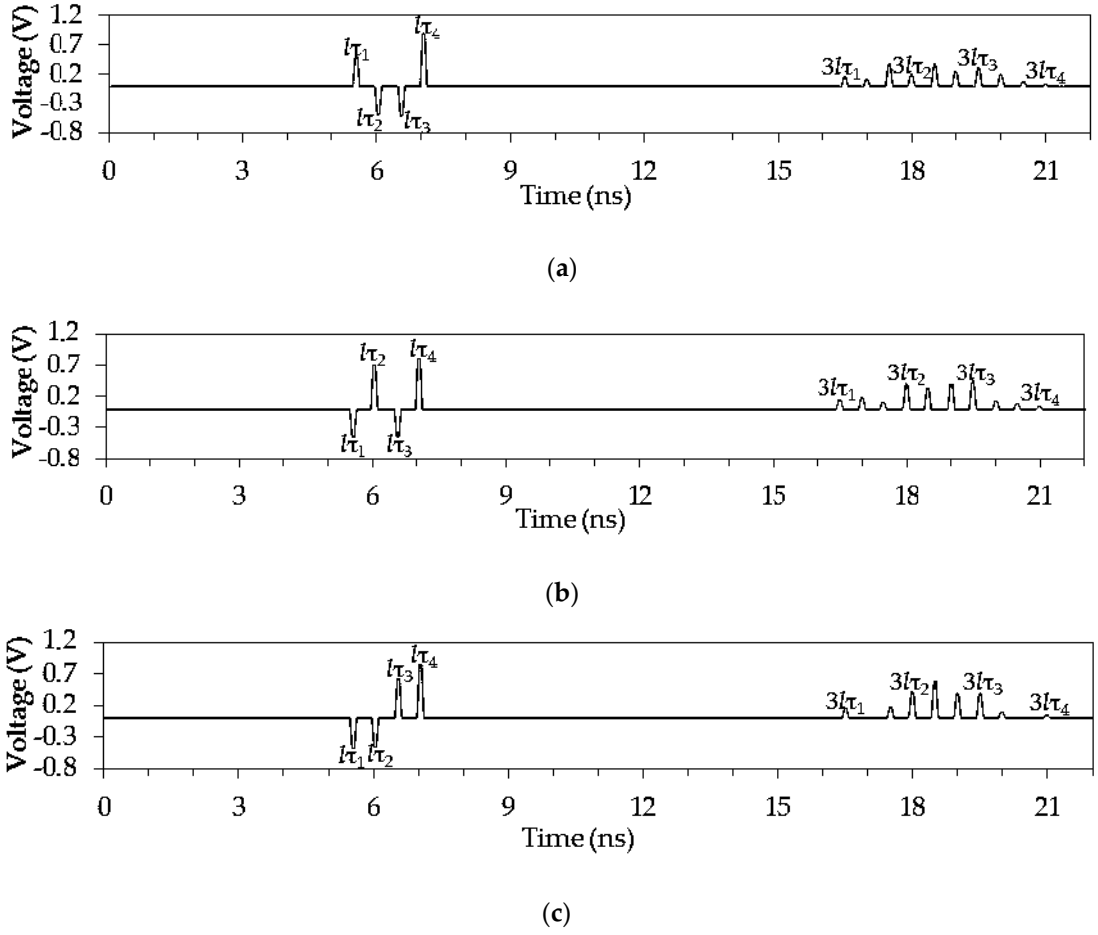

Figure 28. Voltage waveforms at the output of the 3-half-turn circuits with l = 1 m: (**a**) 1, (**b**) 2, and (**c**) 3.

Figure 28 shows one group of pulses in which the delays are proportional to 1 per-unit length delay and the second group of pulses in which the delays are proportional to 3 per-unit length delays. In the first group, 2 pulses with negative polarity are observed at the output of all circuits. There were no such pulses in the time response of the reflection symmetric MF (Figure 22). The maximum amplitudes at the ML output are in the first group of pulses (with a delay of $l\tau_4$) and are equal to 0.81 V and 0.84 V for circuits 1 and 3, respectively.

In the second group of pulses, in addition to the main pulses with delays that are proportional to the per-unit length delays of the modes, we observed some more pulses. For circuits 1 and 2, their number is 6; for circuit 3 it is 4, and their waveforms differ from trapezoidal ones. This may mean that several pulses are overlapped, and consequently, the number of additional pulses is less than the real number. It is also proved to be true by the increase in the total amplitude of some adjacent pulses. To verify this assumption, for all the circuits, the l value is increased from 1 to 8 m. Fragments of the output voltage waveforms (from 130 to 170 ns) for this case are presented in Figure 29.

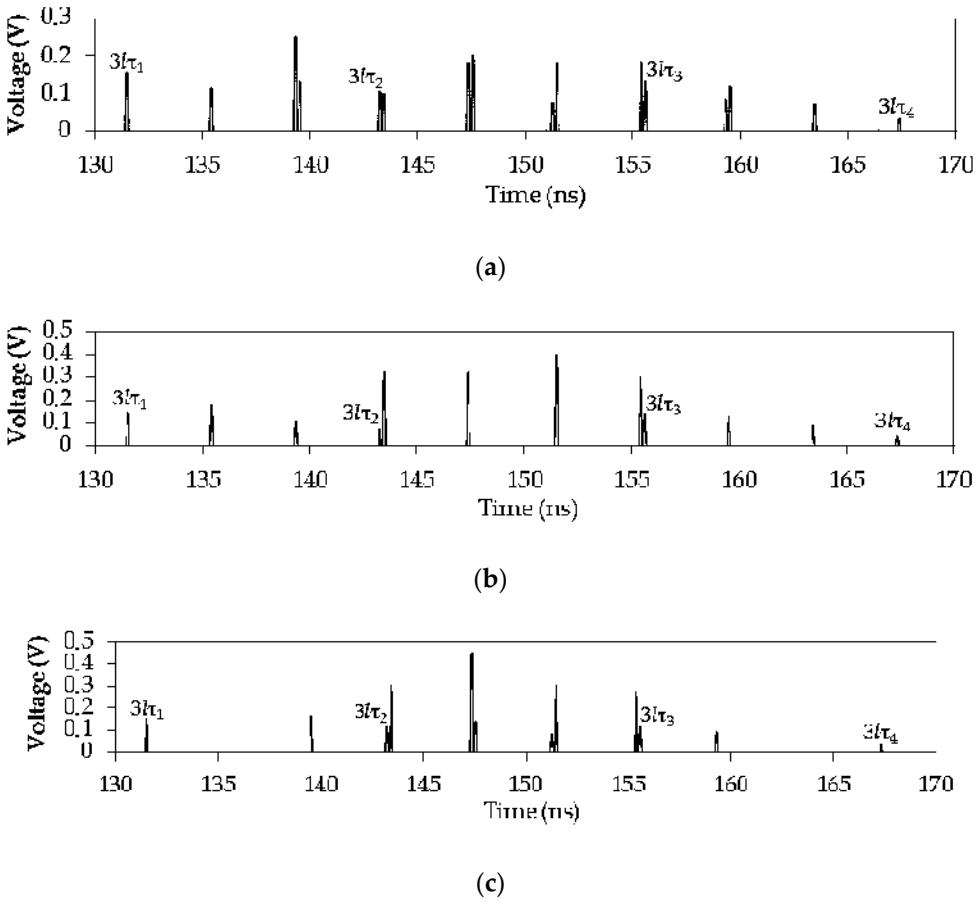

Figure 29. Voltage waveforms at the output of the 3-half-turn circuits: (**a**) 1, (**b**) 2, and (**c**) 3 for l = 8 m.

The results of the simulation confirm the hypothesis discussed above. Additional pulses have increased to 12 for circuit 1 (initially there were 6), to 8 for circuit 2 (initially there were 6), and to 6 for circuit 3 (initially there were 4). However, for circuits 2 and 3, it was not possible to achieve a substantial increase in the time intervals between pulses by increasing the length of the MLs. The maximum pulse amplitude level on the time response of these circuits is greater than that of circuit 1. This means that some pulses superimposed, and as a result, the total amplitude increased. To achieve an increase in time intervals, for circuits 2 and 3, the h values must be increased from 0.5 to 1 mm. Figure 30 shows the output voltage waveforms of circuits 2 and 3.

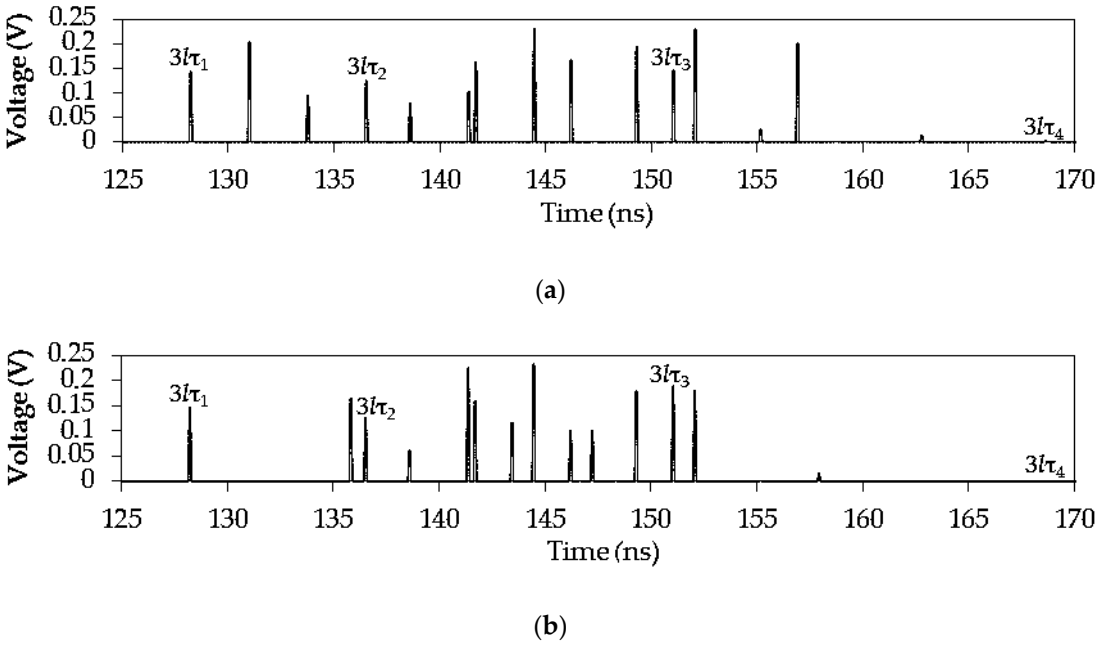

Figure 30. Voltage waveforms at the output of the 3-half-turn circuits with l = 1 m and h = 1 mm: (**a**) 2, (**b**) 3.

Figure 30 demonstrates the complete pulse decomposition in circuits 2 and 3. As well as in circuit 1, there are 12 additional pulses. Table 3 summarizes the delay values of all 16 pulses, both main and additional, for circuit 1 at h = 0.5 mm and for circuit 2 and 3 at h = 1 mm when l = 8 m.

Table 3. Pulse delays 1–16 (ns) for circuits 1, 2, and 3.

No	1	2	3	4	5	6	7	8	9	10	11	12	13	14	15	16
1	131.4	135.3	139.2	139.4	143.1	143.3	147.2	147.4	151.1	155.3	155.3	155.5	159.2	159.4	163.3	167.2
2	128.1	130.9	133.6	136.4	138.5	141.2	141.6	144.3	146.1	149.2	150.96	151.96	155.0	156.8	162.7	168.5
3	128.1	135.7	136.4	138.5	141.2	141.6	143.3	144.3	146.1	147.1	149.2	150.9	151.9	155.0	157.8	168.5

For 2 half-turns configurations (Section 2.3.1), the additional pulse delays were found to be equal to the arithmetic mean of double delays of mode pulses or simply the sum of two delays of the pulses in different combinations. However, this statement is not quite correct for the reflection symmetric ML consisting of 3 half-turns. The analysis of the data in Table 3 and the time responses in Figures 28–30 shows that each additional pulse delay is equal to the arithmetic mean value of the delays of 2 pulses, which can be a combination of both main and additional pulses. For a more detailed analysis, Table 4 summarizes the assumed additional pulse delays at l = 8 m and h = 0.5 mm for circuit 1.

Table 4. Assumed values of the additional pulse delays equal to the arithmetic mean (AM) value of the two modes 1–4 delays for circuit 1.

AM	$3l(\tau_1 + \tau_2)/2$	$3l(\tau_1 + \tau_3)/2$	$3l(\tau_2 + \tau_3)/2$	$3l(\tau_1 + \tau_4)/2$	$3l(\tau_2 + \tau_4)/2$	$3l(\tau_3 + \tau_4)/2$
t, ns	137.287	143.467	149.333	149.353	161.4	155.219

There are no pulses in Figure 29a with the delay values from Table 4. After analyzing Figure 29a in detail, it is clear that the delay values of additional pulses are proportional to the arithmetic mean of the delays of the pair of pulses. For example, the main ones are pulses 1, 5, 12, and 16, while the rest are additional pulses.

Thus, we demonstrated the possibility of decomposing a USP in a reflection symmetric ML of 3 cascaded half-turns. As a result of simulating 3 investigated circuits, additional impulses were found

in the time response. In accordance with the way conductors are connected, the values of additional pulses are proportional to the arithmetic mean value of the 2 pulse delays, which can be a combination of both main and additional pulses.

The maximum amplitudes at all ML circuits output is in the first group of pulses with a delay of τ_4. As in Section 2.3.1, it is possible to optimize the reflection symmetric ML by the criterion of equalization of time intervals between decomposition pulses, including between additional ones. Such optimization can lead to more effective protection against USPs. However, only 2 instead of 6 resistors are required at the ends of passive conductors. In addition, the input and output of MLs are at different ends of the line (as opposed to the structures of 2 half-turns), which in practice can be effectively implemented.

2.3.3. Reflection Symmetric Meander Line of 4 Cascaded Half-Turns

We now investigate reflection symmetric MLs in which the signal travels a distance $4l$ (4 cascaded half-turns). The circuits under study are shown in Figure 31.

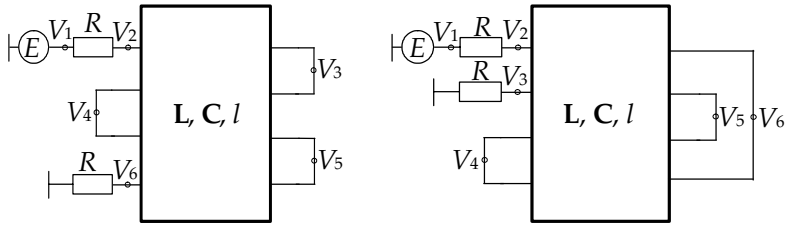

Figure 31. Equivalent circuits of connecting 4 half-turn reflection symmetric ML: (**a**) 1, (**b**) 2.

The construction of a geometric model of the cross-section with optimal values of the parameters (s = 0.51 mm, w = 1.6 mm, t = 0.018 mm, h = 0.5 mm, ε_r = 4.5), as well as the calculation of the time response, was performed similarly to the construction shown in Section 2.3.1. The output voltage waveforms were obtained (nodes V_6 in Figure 31a and V_3 in Figure 31b), and these are presented in Figure 32, respectively.

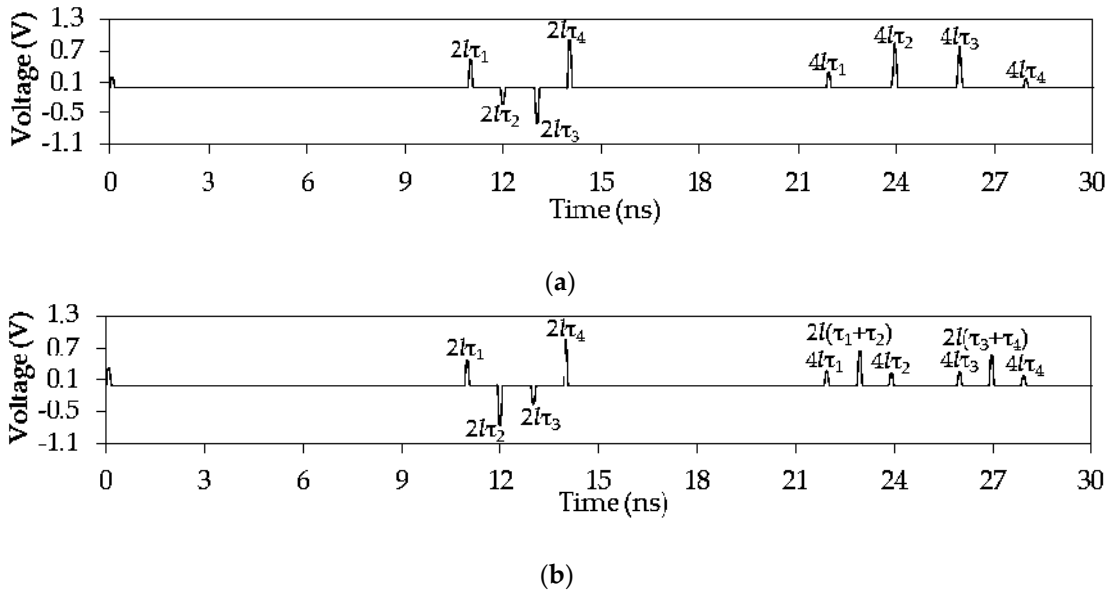

Figure 32. Voltage waveforms at the output of the 4-half-turn circuits with l = 1 m: (**a**) 1 and (**b**) 2.

On the obtained voltages waveforms, two groups of pulses are observed, the delays of which are proportional to 2 and 4 per-unit length delays, respectively. As in Section 2.3.2, pulses of modes 2

and 3 of negative polarity are observed in the first group. The appearance of such pulses is explained by the fact that at the right end of the circuit, the pulses are reflected by bridges. In the circuit of the reflection symmetric MF, all ends of the conductors have resistors that improve the matching of each mode. Whereas the presence of bridges in the reflection symmetric ML leads to an SC for some modes and an OC for other modes.

In the other group of pulses, in addition to the main pulses with delays, which are proportional to 4 delays for circuit 2, additional pulses are observed, with different delays. It is possible that such pulses can also be observed in circuit 1. This can be confirmed by the fact that the amplitude of the modes 2 and 3 pulses (with delay values of $4l\tau$) increases on its own. To achieve an increase in the time intervals, for circuit 1, the l value must be increased from 1 to 8 m. Figure 33 shows a fragment of the output voltage waveforms (from 175 to 225 ns).

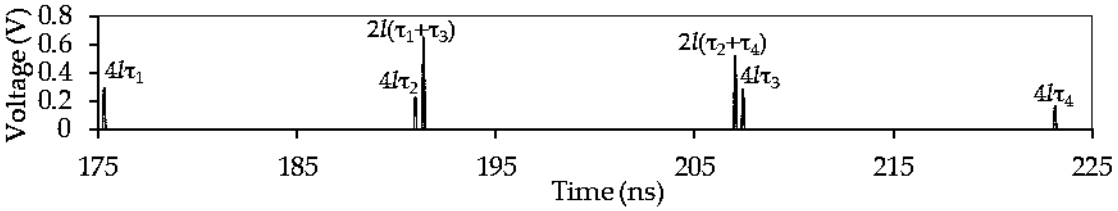

Figure 33. Voltage waveforms at the output of the 4-half-turn circuit 1 with l = 8 m.

The simulation results confirm the assumption that additional pulses do appear in circuit 1. Table 5 summarizes the values of per-unit length delays of the main pulse (modes 1-4). Table 2 also shows values of per-unit length delays that are multiplied by 2, 4, and 32, because the delays of main pulses at the output of the reflection symmetric ML are multiples of 2, 4 (l = 1 m), and 32 (l = 8 m) per-unit length delays.

Table 5. Per-unit length delays (ns/m) for modes 1–4, multiplied by 1, 2, 4, and 32.

Multiplier	1	2	3	4
1	5.4698	5.9591	6.4746	6.9687
2	10.9398	11.9183	129.493	13.9376
4	21.8795	23.8366	258.987	27.8752
32	175.036	190.693	207.189	223.001

The analysis of the data in Table 5 and the time responses in Figures 32 and 33 show that the additional pulse delay values are equal to the arithmetic mean of the delays that are multiples of four per-unit length delays multiplied by l. Thus, for circuit 1, these delays are equal to $l(4\tau_1 + 4\tau_3)/2 = 2l(\tau_1 + \tau_3) = 23.8891$ ns and $l(4\tau_2 + 4\tau_4)/2 = 2l(\tau_2 + \tau_4) = 25.8559$ ns, and for circuit 2, they are equal to $l(4\tau_1 + 4\tau_2)/2 = 2l(\tau_1 + \tau_2) = 22.85805$ ns and $l(4\tau_3 + 4\tau_4)/2 = 2l(\tau_3 + \tau_4) = 26.88695$ ns. The values obtained are exactly the same as those obtained in the time response simulations.

In addition, Figure 32 shows that the first pulse with a delay value of zero is crosstalk. Its amplitude is lower than that of the decomposition pulses. It shows that increasing the crosstalk amplitude can reduce the amplitude of the decomposition pulses. This can be implemented by optimization based on the criterion of pulse amplitude equalization. It is clear that the reflection symmetric ML should be optimized independently, although it is based on the reflection symmetric MF with optimal cross-section parameters. Furthermore, due to the equalized time intervals between the decomposition pulses, no additional pulses in the reflection symmetric MF are observed in circuit 1. In this way, it is necessary to optimize the reflection symmetric ML (similar to the schemes shown earlier), by the criteria of aligning the time intervals between all (main and additional) decomposition pulses and minimizing the voltage amplitude at the circuits output to improve the efficiency of protection against USPs. With regard to attenuation in these cases, the smallest output amplitude of all considered circuits

is about 0.9 V, which is determined by the amplitude of the pulse with a delay of $2\tau_4$. Finally, it is important to note that this 4 half-turn case does not require resistors at all.

Thus, the results of the study of a reflection symmetric ML of various circuit designs are presented for the configurations with 2, 3, and 4 cascaded half-turns. In these circuits, additional pulses were detected in the time response at the line output, whereas previously, in the reflection symmetric MF and the turn of the symmetric ML, they were not detected. It is demonstrated that the additional pulse delays are equal to the arithmetic mean value of an integer number of per-unit length mode delays in different variants. However, such pulses may be hidden. The detection of additional pulses in the output signal is important, since the maximum amplitude for all circuits is determined precisely by the amplitude of the additional pulses. Moreover, the additional pulse delays can overlap both between themselves and with the main pulses, which can lead to a significant increase in the maximum amplitude, and as a result, to a decrease in attenuation.

2.4. Modal Filter with a Passive Conductor in the Reference Plane Cutout

For the study, we chose a simple asymmetric structure of the MF, whose design is formed by means of two cutouts in the ground plane of the ordinary MSL, which form a passive conductor between themselves. Figure 34a shows the geometric model of the cross-section of the MF, where w_1, w_2, and w_3 are the widths of the conductors, s_1 and s_2 are the separations of the conductors, and h is the thickness of the dielectric. As the dielectric material, we selected fiberglass ($\varepsilon_r = 4.5$).

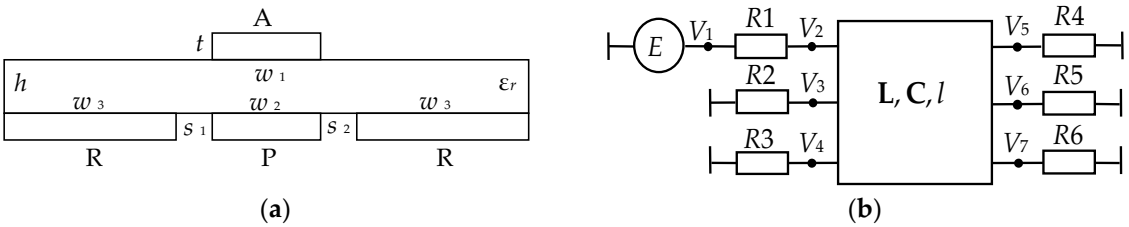

Figure 34. (**a**) Cross-section and (**b**) equivalent circuit of the MF. The conductors: A—active, P—passive, R—reference.

The equivalent circuit of the MF is shown in Figure 34b. The active conductor is connected to an EMF source E and internal resistance R_1. At the other end of this conductor is located the load R_4. The values of R_1, R_2, R_4, and R_5 are assumed to be equal to 50 Ω, and $R_3 = R_6 = 1$ mΩ for connecting the extreme conductors. The excitation is a trapezoidal pulse with the EMF amplitude of 2 V, the rise time is 150 ps, the flat top time is 200 ps, and the fall time is 150 ps. Losses were not taken into account.

2.4.1. Simulation of the Symmetrical Structure of an MF with a Passive Conductor in the Reference Plane Cutout

The simulation of a symmetrical (relative to the vertical axis) structure was performed with the typical fiberglass parameters ($t = 35$ μm, $h = 0.18$ mm for the MF length of $l = 1$ m) with weak coupling between A and P conductors ($w_1 = w_2 = w_3 = 1$ mm and $s_1 = s_2 = 0.5$ mm), and with strong coupling ($w_1 = w_2 = 3.5$ mm, $w_3 = 0.5$ mm, and $s_1 = s_2 = 3.0$ mm) between them. For further simplicity, we will refer to them as MF1 and MF2, respectively. The influence of the boundary conditions at the ends of the passive conductor was simulated as follows: SC–OC, OC–SC where the SC was set with a resistance of 10^{-6} Ω, and the OC was 10^9 Ω.

Figures 35 and 36 show the results of simulating the output voltage waveforms of MF1 and MF2. Figure 35b,c, and Figure 36b,c show that the change in the boundary conditions results in the appearance of 2 additional pulses of negative polarity and different delay values between 2 pulses with a triple path along the line ($3l\tau_1$ and $3l\tau_2$). The amplitude of these pulses is greater than the amplitude of the mode pulses. The delay values for main pulses, their reflections, and additional modal pulses are given in Table 6. The amplitudes of the main and additional pulses are summarized in Table 7.

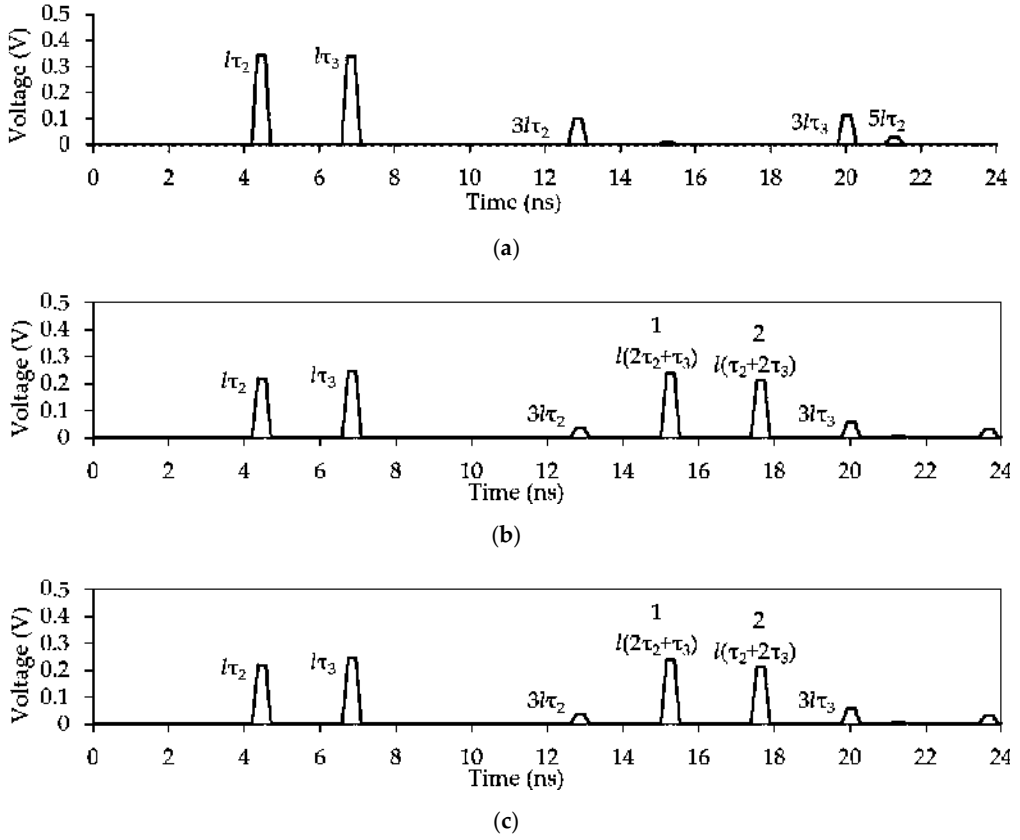

Figure 35. Voltage waveforms at the MF1 output for (**a**) $R2 = R5 = 50\ \Omega$, (**b**) OC–SC, and (**c**) SC–OC.

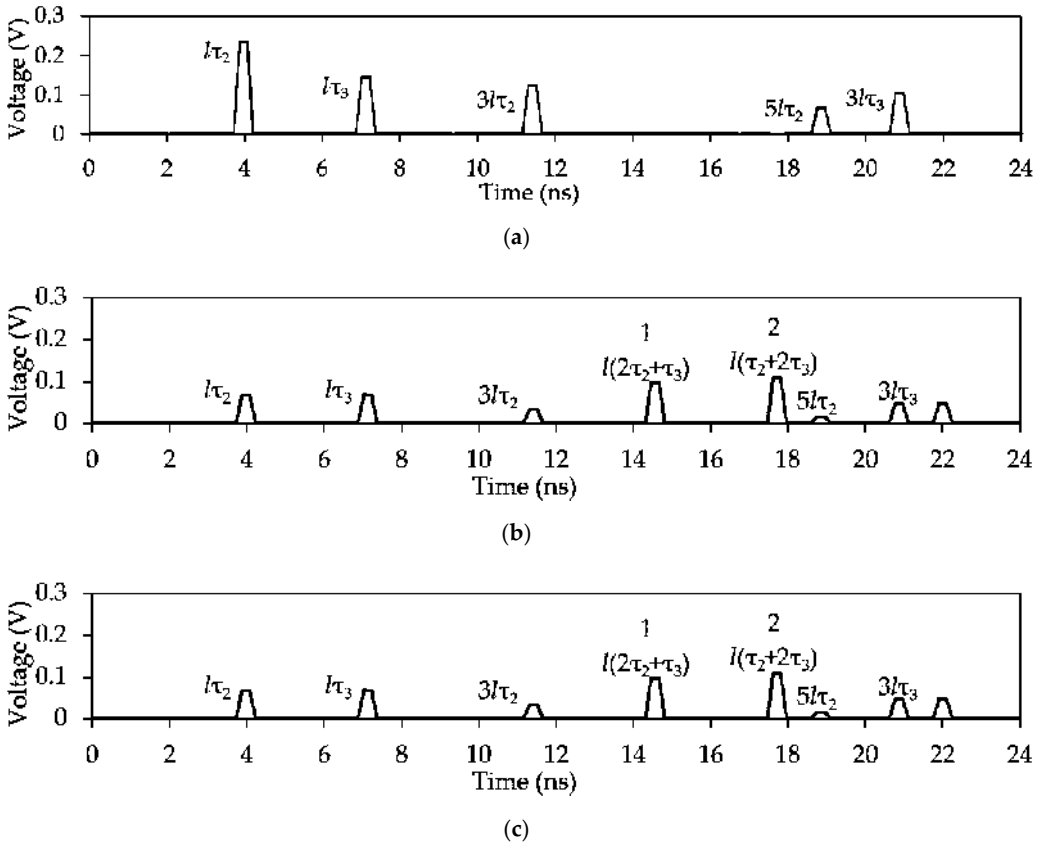

Figure 36. Voltage waveforms at the MF2 output for (**a**) $R2 = R5 = 50\ \Omega$, (**b**) OC–SC, and (**c**) SC–OC.

Table 6. Delays (ns) of the main and additional pulses.

	$l\tau_1$	$l\tau_2$	$l\tau_3$	$3l\tau_1$	$3l\tau_2$	$3l\tau_3$	$2l(\tau_2 + \tau_3)$	$l(\tau_2 + 2\tau_3)$
MF1	3.95	4.21	6.60	11.86	12.62	19.77	15.00	17.39
MF2	3.67	3.72	6.87	11.03	11.16	20.61	14.30	17.46

Table 7. Amplitudes (V) of 4 main and 2 additional pulses at the output of MF1 and MF2 for OC–SC and SC–OC.

R2-R5	MF1						MF2					
OC–SC	0.23	0.26	0.038	0.062	0.25	0.21	0.069	0.070	0.040	0.023	0.104	0.112
SC–OC	0.22	0.25	0.042	0.064	0.24	0.22	0.071	0.071	0.037	0.023	0.111	0.101

It is noteworthy that in the symmetrical structure of the MF with the passive conductor in the cutout of the reference plane, the pulse of the first mode does not manifest itself. As for additional pulses, they only appear when the boundary conditions at the ends of the passive conductor change.

2.4.2. Simulation of the Asymmetric MF Structure with a Passive Conductor in the Reference Plane Cutout

At this research stage, the asymmetry effect was considered for MF2, because strong coupling results in a greater attenuation of a USP. The asymmetry was obtained by reducing s_1 from 3.5 to 0.5 mm at s_2 = 3.5 mm, i.e., by placing of one of the reference conductors closer to the other.

Figure 37 shows examples of the results of simulating the voltage waveforms at the output of the MF2 for l = 1 m. Figures 37b and 38c show the appearance of 2 additional pulses of negative polarity with other values of delays between 2 pulses with a triple path through the line ($3l\tau_1$ and $3l\tau_2$). Thus, at s_1 = 0.5 mm there are two of them, which are clearly expressed (Figure 37c); for s_1 = 1.1 mm, there is one (Figure 37b); and for s_1 = 3.5 mm, when the MF structure is completely symmetric, there are not any (Figure 37a). Analyzing Figure 37, it can be concluded that the appearance of additional pulses is affected by the asymmetry of the MF structure.

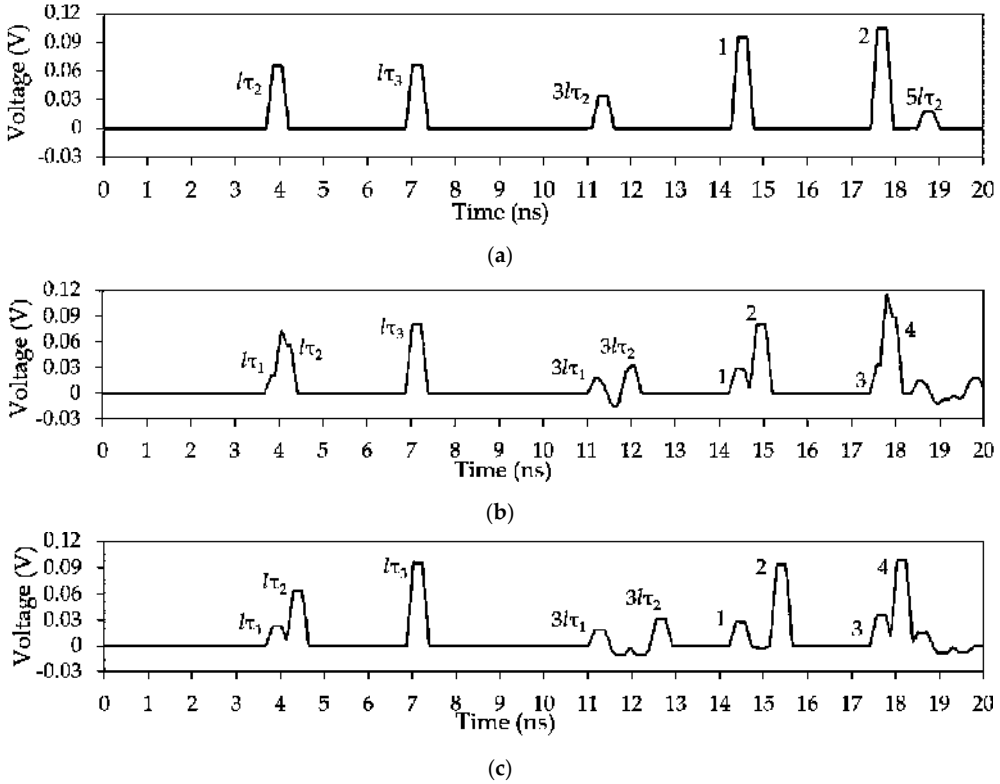

Figure 37. Voltage waveforms at the MF output for (**a**) s_1 = 3.5, (**b**) 1.1, (**c**) 0.5 mm, and l = 1 m.

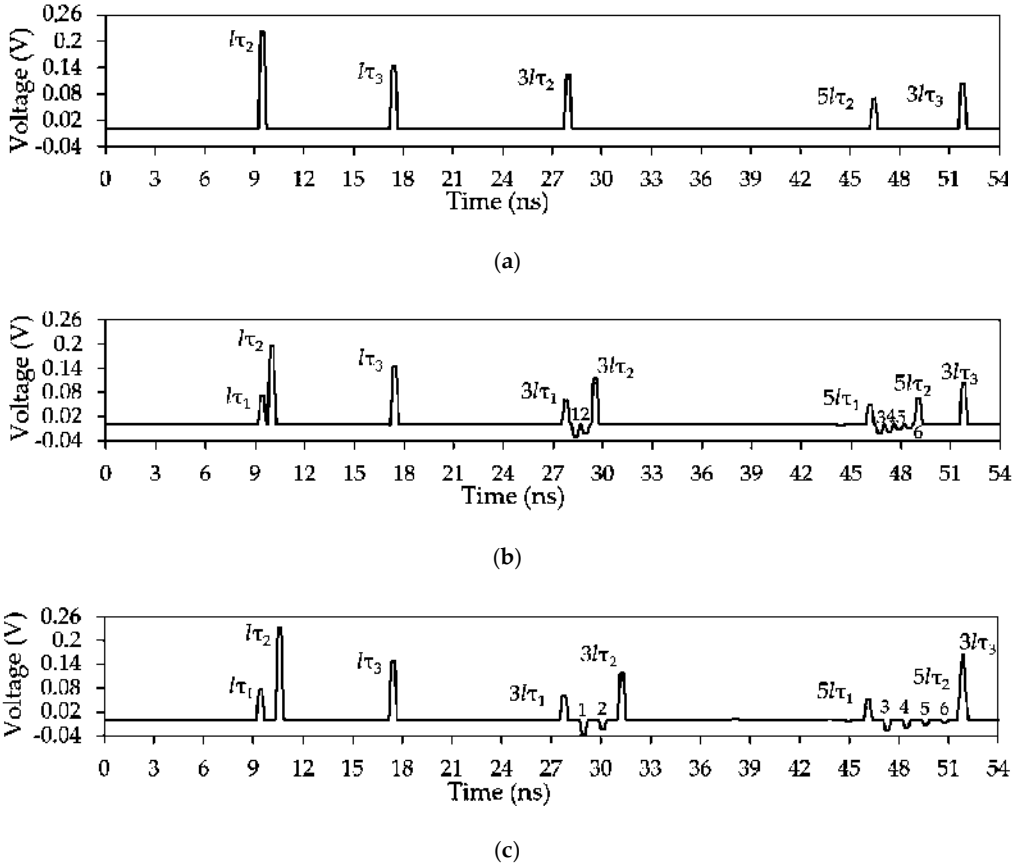

Figure 38. Voltage waveforms at the MF output (**a**) s_1 = 3.5, (**b**) 1.1, (**c**) 0.5 mm, and l = 2.5 m.

Since at l = 1 m it is complicated to determine the exact arrival time of additional pulses (due to their partial overlap with the main modes), the line length was increased to 2.5 m. Tables 8 and 9 show the values of per-unit length delays and arrival times for mode pulses. The waveforms of the output voltage are shown in Figure 38. Table 10 shows the resulting combinations and the arrival times of additional pulses 1–6. The analysis of Figure 38 and Table 10 allows us to conclude that with the increase in s_1, the time intervals between additional pulses and the amplitude become smaller: for s_1 = 0.5 mm, the interval is 1.162 ns and the amplitude is 0.38 V, but for s_1 = 1.1 mm, they are 0.588 ns and 0.28 V. Reducing the intervals and the amplitude leads to the disappearance of pulses, which is confirmed by Figure 38a when they disappear at s_1 = 3.5 mm. It is also seen that their number increases by two (at $3l\tau$, there are 2 additional pulses, but at $5l\tau$, there are 4 of them), and the pulse amplitudes decrease.

Table 8. Per-unit length mode delays (ns/m).

s_1, mm	τ_1	τ_2	τ_3
3.5	3.658	3.695	6.872
1.1	3.670	3.906	6.872
0.5	3.670	4.135	6.872

Table 9. Arrival times (ns) for mode pulses.

s_1, mm	$l\tau_1$	$l\tau_2$	$l\tau_3$	$3l\tau_1$	$3l\tau_2$	$3l\tau_3$	$5l\tau_1$	$5l\tau_2$	$5l\tau_3$
3.5	9.145	9.237	17.181	27.43	27.712	51.543	45.726	46.187	85.905
1.5	9.176	9.764	17.181	27.529	29.292	51.543	45.883	48.821	85.905
0.5	9.176	10.338	17.181	27.528	31.014	51.541	45.879	51.691	85.903

Table 10. Arrival times (ns) for additional pulses.

№	1	2	3	4	5	6
Combination	$l(2\tau_1 + \tau_2)$	$l(\tau_1 + 2\tau_2)$	$l(4\tau_1 + \tau_2)$	$l(3\tau_1 + 2\tau_2)$	$l(2\tau_1 + 3\tau_2)$	$l(\tau_1 + 4\tau_2)$
s_1 = 1.1 mm	28.117	28.705	46.471	47.059	47.647	48.235
s_1 = 0.5 mm	28.69	29.852	47.041	48.203	49.365	50.527

The influence of the boundary conditions on the «beginning-end» of a passive conductor was simulated as SC–OC and OC–SC. To save space, the results are given only for the OC–SC, as the largest attenuation of the input signal occurs in this mode. It shows that as the asymmetry increases and boundary conditions change, more additional pulses appear: at s_1 = 3.5 mm (Figure 39a) there are 2 of them, and at s_1 = 1.1 (Figure 39b) and 0.5 mm (Figure 39c), there are 4 of them. Figure 40 shows the results of simulating the voltage waveforms at the MF output for s_1 = 3.3; 1.1; 0.5 mm. In Figure 39, 2 pulses are observed (in Figure 40a, they are designated as 1, 2, and in Figure 39b, they are designated as 2, 4, because there are 2 more pulses), the amplitudes of which are greater than the amplitudes of the pulses of the 3 modes. Figure 39b,c show that with increasing asymmetry, the interval between the additional pulses 1 and 2, as well as 3 and 4, becomes larger. In addition, weakly expressed additional pulses of negative polarity appear between pulses $3l\tau_1$ and $3l\tau_2$ (Figure 39b,c) (as discussed above).

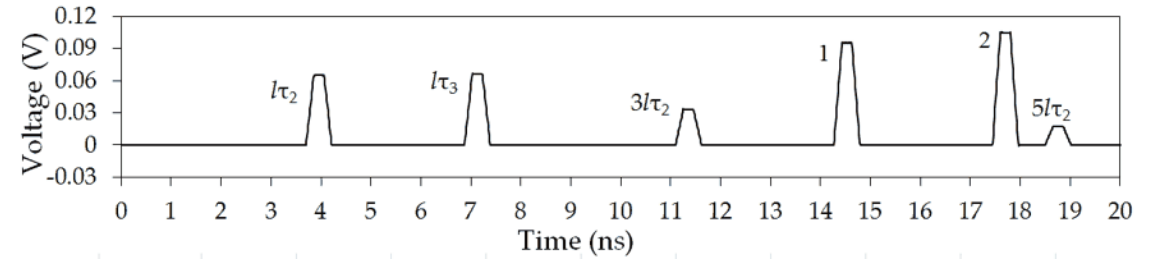

(**a**)

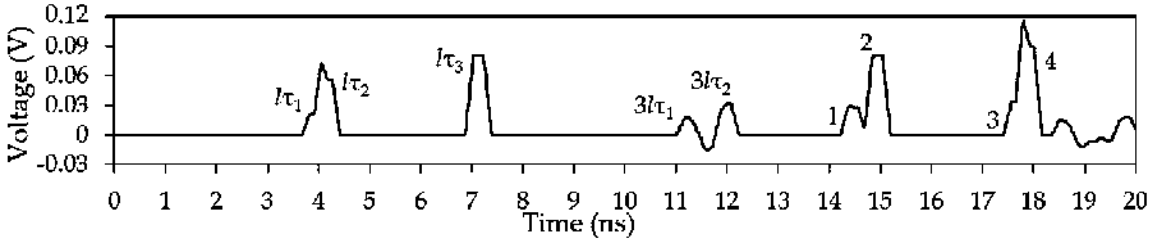

(**b**)

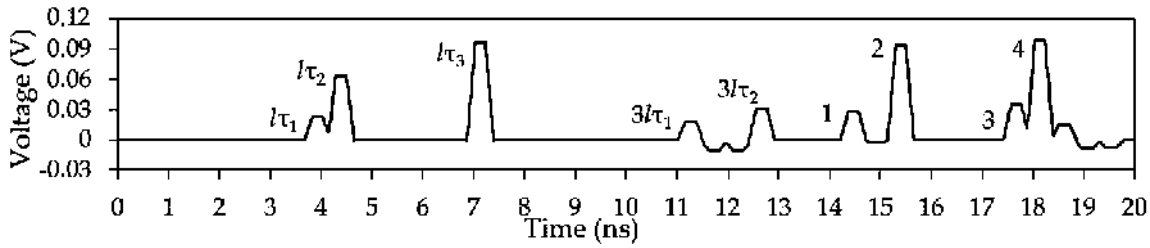

(**c**)

Figure 39. Voltage waveforms at the MF output with OC–SC on the passive conductor for (**a**) s_1 = 3.5, (**b**) 1.1, (**c**) 0.5 mm, and l = 1 m.

Figure 40 shows the dependence of the maximum amplitude of additional pulses 2 (in Figure 39a) and 4 (in Figure 39b,c) on s_1. At s_1 = 0.7 mm, the minimum amplitude of 0.096 V is achieved.

After s_1 = 0.9 mm, the amplitude increases sharply, which is explained by the merge of pulses with the summation of their amplitudes. After s_1 = 1.5 mm, the amplitude decreases monotonically to 0.105 V. The pulse merge is confirmed by Figure 39, where 2 pulses are clearly visible for s_1 = 3.5 mm, and 4 pulses are visible for s_1 = 1.1 and 0.5 mm. Thus, the asymmetry of the MF with the optimal s_1 value makes it possible to minimize the maximum of the amplitudes of additional pulses.

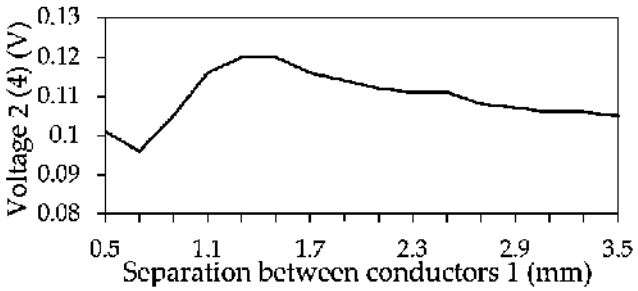

Figure 40. Dependence of the output voltage amplitude on s_1.

Thus, it is established that the appearance of additional pulses in the MF with the passive conductor in the cutout of the reference plane has a strong influence of changing boundary conditions at the ends of the passive conductor. The maximum amplitude of these pulses is greater than the maximum amplitude of the basic mode pulses. In addition, the introduction of asymmetry has a significant influence. Thus, when the value of s_1 decreases, a group of pulses of negative polarity appears. As the value of s_1 increases, the time intervals between the additional pulses and their amplitudes become smaller, resulting in the disappearance of the additional pulses. A change in the boundary conditions with decreasing s_1 allowed us to reduce the amplitude of additional pulses.

2.4.3. Experimental Confirmation of Additional Pulses

The results of field and computational experiments were compared using 2 approaches: quasistatic, based on the method of moments [18,19], and electrodynamic, based on the finite integration method [20]. The simulations took into account losses in conductors and dielectrics. In the quasistatic approach, for the segmentation of boundaries, we assumed that there are 5 segments on the edges of conductors, which provides a good accuracy of results. In the electrodynamic approach, the structure under study was divided into cells with a minimum size of 11.6 μm. FR-4 fiberglass was selected as a dielectric material. The values of relative permittivity ε_r and dielectric loss tangent tgδ at a frequency of 1 MHz were 4.5 and 0.018, respectively.

The simulation of the influence of the boundary conditions influence at the beginning and the end of a passive conductor was carried out as SC–OC and OC–SC, where the SC was set with a resistance of 10^{-6} Ω, and the OC was set with a resistance of 10^9 Ω. As an excitation pulse in the simulation, we used a digitized signal of the oscillograph utilized in the field experiment. The pulse had an amplitude of 0.284 V and rise and fall times (by the levels 0.1–0.9) of 0.32 and 0.22 ns, respectively (Figure 41). The total pulse duration, by the level of 0.5, was 0.18 ns.

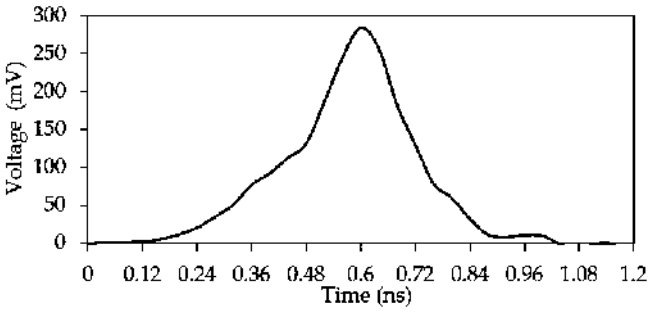

Figure 41. Digitized signal of the oscilloscope.

We performed the tracing of PCB layouts for configurations MF1 and MF2. The lengths of the MFs were 300 mm, and the dimensions of the PCBs were 125 mm, so the MFs were made in the form of a meander. To reduce the coupling of the turns on each other, we chose an increased distance of $5w$ between them. The layout tracing is shown in Figures 42 and 43.

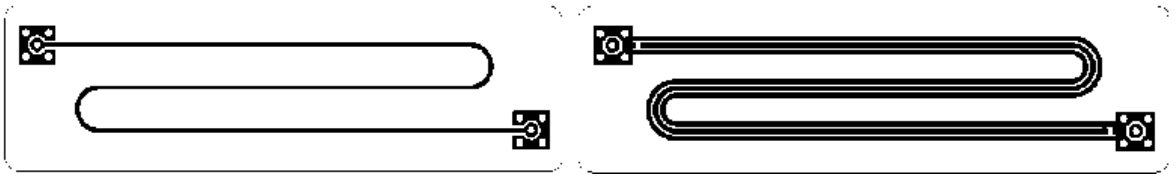

(**a**) (**b**)

Figure 42. Photomasks of the MF1 layout: (**a**) top and (**b**) bottom layers.

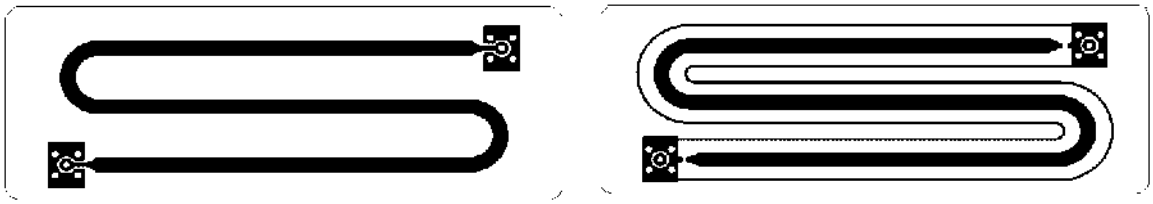

(**a**) (**b**)

Figure 43. Photomasks of the MF2 layout: (**a**) top and (**b**) bottom layers.

To install SMA connectors, we chose contact pads (CP) with dimensions: 8 × 8 mm for MF1 and 8 × 12 for MF2. In each CP, there are 5 vias with a diameter of 1.2 mm designed to connect conductors on different layers of a PCB. For matching, resistors of a standard size 1206 with a resistance of 50 Ω were used. To mount resistors, CPs of 1.7 × 1.25 mm were installed at the ends of the passive conductors (they are the same for two MFs). The manufactured layouts are shown in Figures 44 and 45.

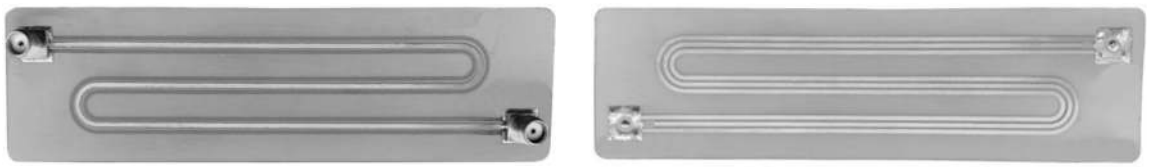

(**a**) (**b**)

Figure 44. Photos of the MF1 layout: (**a**) top and (**b**) bottom layers.

(**a**) (**b**)

Figure 45. Photos of the MF2 layout: (**a**) top and (**b**) bottom layers.

After manufacturing the MF, thegeometric parameters were checked. The widths of the printed conductors were controlled using a magnifying glass with a measuring ruler and the thicknesses of the dielectric and conductors were measured using a mechanical micrometer. The real values of the geometric parameters were obtained, the average values of which for MF1 were h = 0.18 mm,

t = 0.033 μm, and $w_1 = w_2 = w_3$ = 1 mm; for MF2, they were h = 0.18 mm, t = 0.033 μm, $w_1 = w_2$ = 3.5 mm, and w_3 = 0.5 mm.

To conduct the field experiment in the time domain, we used a setup whose structural diagram is shown in Figure 46. For the required accuracy of signal registration, the horizontal and vertical paths of the measuring system were calibrated. The measurement accuracy of instantaneous values of pulse signals in amplitude was ±3%, and time intervals at a given sweep were ±2%.

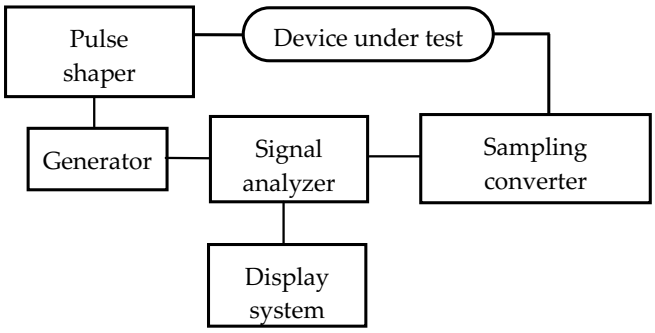

Figure 46. Experimental setup diagram for the time domain.

Figures 47 and 48 show the results of field and computational experiments for MF1 and MF2, respectively.

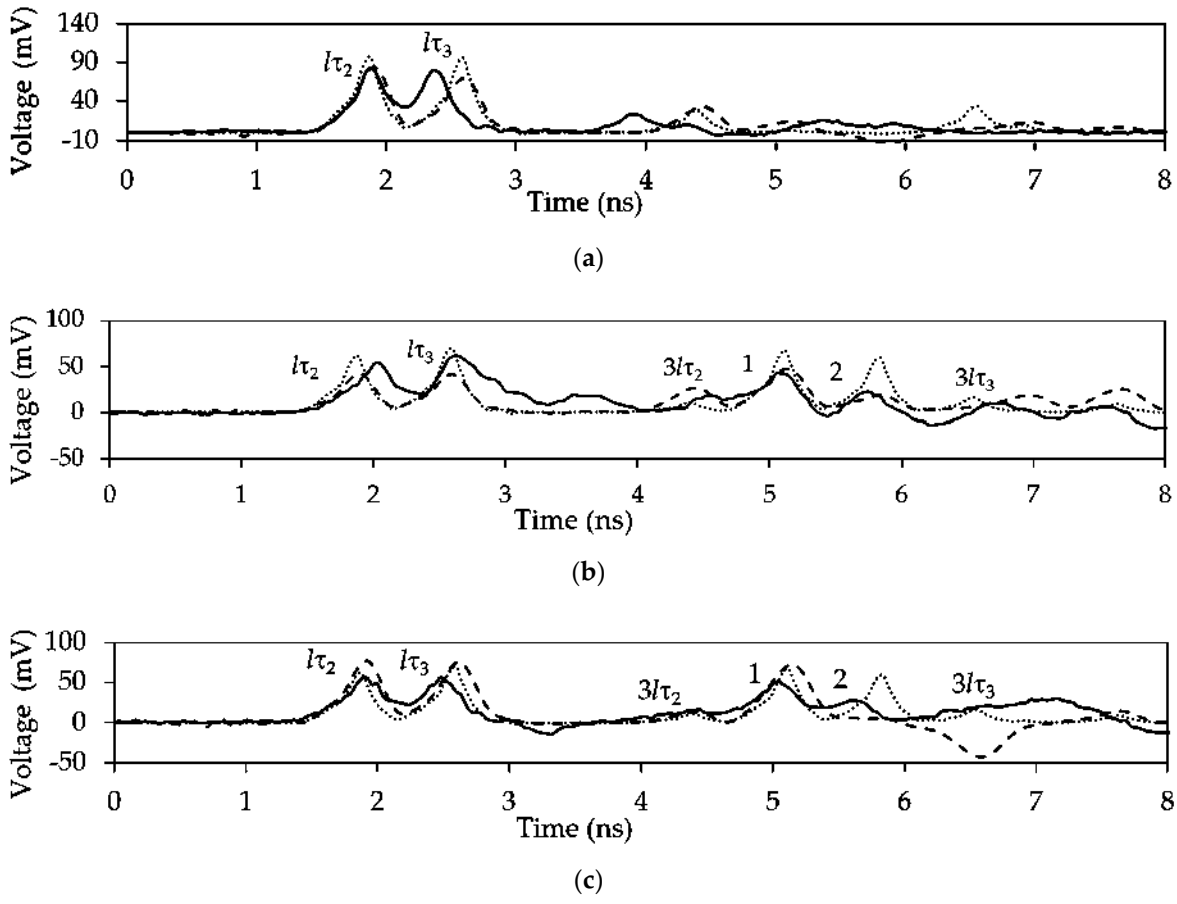

Figure 47. Voltage waveforms at the MF1 output obtained during the experiment (—-), electrodynamic (– –) and quasistatic (····) simulations for (**a**) $R2 = R5$ = 50 Ω, (**b**) OC–SC, and (**c**) SC–OC.

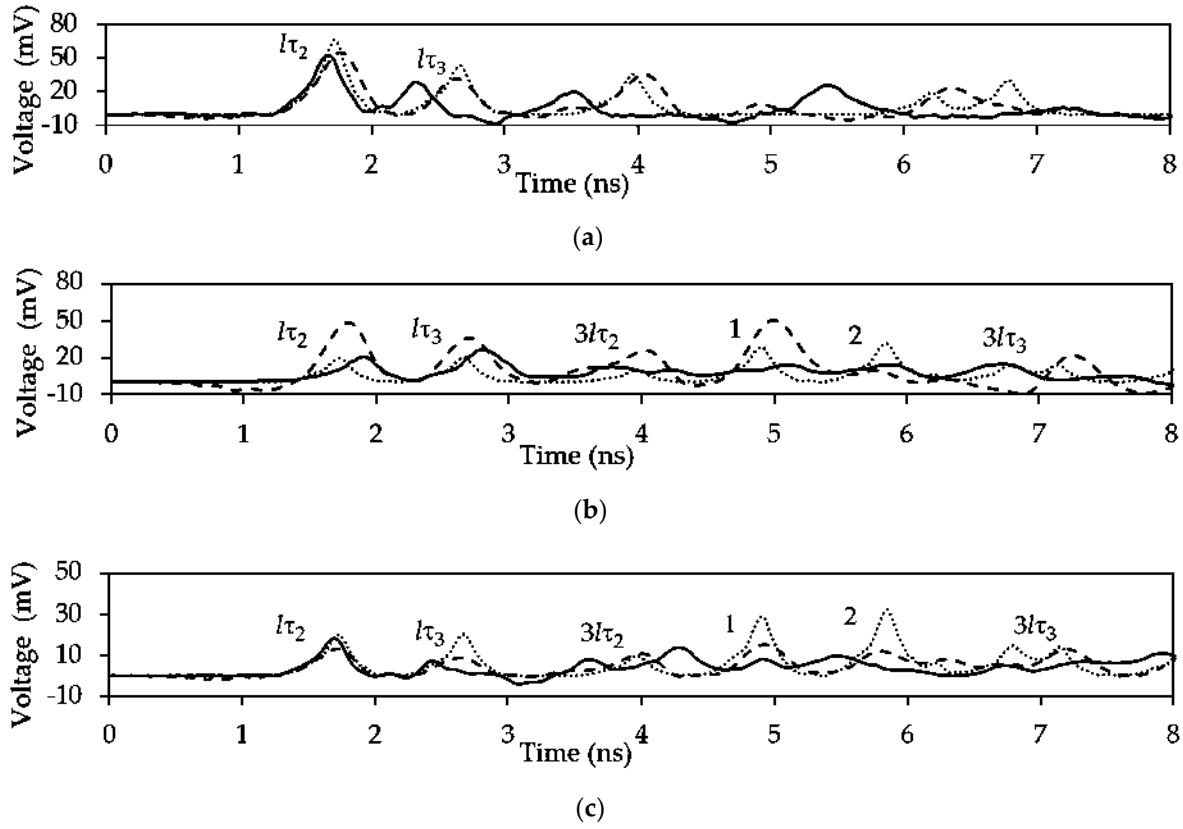

Figure 48. Voltage waveforms at the MF2 output obtained during the experiment (—-), electrodynamic (– –) and quasistatic (····) simulations for (**a**) $R2 = R5 = 50\ \Omega$, (**b**) OC–SC, and (**c**) SC–OC.

The detailed analysis of Figures 47 and 48 showed the presence of additional pulses (designated as 1 and 2), which appear when the boundary conditions at the ends of the passive conductor change. From Figure 47b,c we can see that the amplitude of the additional pulse 1 is greater than 2. The analysis of Figure 48b,c also showed 2 additional pulses but with lower amplitudes. Tables 11 and 12 show the amplitude of additional pulses 1 and 2 according to the results of both the simulations and the experiment. In general, the amplitudes of additional pulses are comparable to the amplitudes of mode pulses.

Table 11. Amplitudes (mV) of additional pulses 1 and 2 at the output of MF1 obtained with various types of analysis.

Pulse	Quasistatic		Electrodynamic		Experiment	
	OC–SC	SC–OC	OC–SC	SC–OC	OC–SC	SC–OC
1	67	67	47	72	43	51
2	59	59	18	-	22	18

Table 12. Amplitudes (mV) of additional pulses 1 and 2 at the output of MF2 obtained with various types of analysis.

Pulse	Quasistatic		Electrodynamic		Experiment	
	OC–SC	SC–OC	OC–SC	SC–OC	OC–SC	SC–OC
1	28	27	47	15	10	8
2	32	28	9	12	13	10

Despite the fact that the shapes of the additional pulses are in good agreement, it is difficult to estimate the exact time of their arrival, as they partially overlap because of dispersion. To accurately track the dependence of the appearance of additional pulses, we calculated the per-unit length delays, and the arrival times of all pulses were calculated using quasistatic simulation. The results are shown in Table 13.

Table 13. Per-unit length mode delays (ns/m) and arrival times of mode pulses and additional pulses (ns).

	τ_1	τ_2	τ_3	$l\tau_1$	$l\tau_2$	$l\tau_3$	$3l\tau_1$	$3l\tau_2$	$3l\tau_3$	$l(2\tau_2+\tau_3)$	$l(\tau_2+2\tau_3)$
MF1	3.98	4.23	6.58	1.17	1.24	1.88	3.58	3.81	5.92	4.51	5.22
MF2	3.69	3.73	6.86	1.11	1.12	2.06	3.32	3.36	6.18	4.30	5.24

Thus, the results of the experiment confirm the appearance of additional pulses, which earlier was evidenced only in simulation. The amplitude of additional pulses becomes less when the coupling between conductors increases, and the additional pulse delays are determined by a linear combination of the per-unit length delays of the line modes multiplied by the line length.

2.5. Method for Detecting Additional Pulses in the Time Response of Structures with Modal Decomposition

As a result of a stepwise simulation of the circuits of the reflection symmetric MLs as well as any other structures, the general idea about possible conditions of appearance of additional pulses was obtained. On the basis of it, the method for their detecting was formulated. It includes 5 main points which can be supplemented by the characteristics of a specific structure under study:

1. Set a high number of time samples for the pulse repetition period. This will result in a more correct display of time responses (excluding unphysical pulses caused by coarse time discretization).
2. Evaluate in detail the waveforms of the decomposition pulses. Their difference from a trapezoid waveform can suggest the possible overlapping of several pulses.
3. Increase the length of the structure or reduce the duration of excitation by 5–10 times. This enables increasing the values of time intervals between decomposition pulses.
4. Change the parameters of the cross-section. As a result of the symmetry of some structures, the delays of additional pulses can coincide (both among themselves and with the main pulses). In the general case, changing the cross-sectional parameters will allow changing the coupling between the active and passive conductors. This can lead to an increase of time intervals between decomposition pulses.
5. Change the boundary conditions at the ends of the passive conductors from 50 Ω to an SC and OC to the ground or between the conductors.

The importance of this method lies in the fact that in symmetric structures or in structures with optimal cross-sectional parameters, it is sometimes impossible to observe additional pulses. Nevertheless, it is relevant because the maximum amplitude at the output of the investigated structures is determined by the amplitude of the main pulses together with their overlapping with additional pulses. It is a new resource for optimization, and as a consequence, for increasing the efficiency of protective characteristics of such devices.

3. Discussion

As a result of the study, it was found that additional pulses appear in all the structures presented, with the exception of the structure with double MR, and they prove to be an additional resource for reducing the amplitude of the USP. It was shown that the appearance of additional pulses in protective structures with modal decomposition is associated with asymmetry (of cross-section, boundary conditions, and possibly excitation). We note that earlier, when simulating matched MF structures,

such pulses have not been observed, since all ends of the conductors had resistive terminations to the reference ground with the same nominal value, which improves the matching of all modes, while resistor-free designs (for example, using bridges between conductors of an MF) lead to a change in the wave impedance for some modes. Consequently, the appearance of additional pulses is associated with the propagation of waves with different velocities in opposite directions. The delays of such pulses are determined by various linear combinations of the per-unit length delays of the line modes; in particular, they can be equal to the arithmetic mean of the double delays of the even and odd mode pulses (or simply the sum of the delays). It was also revealed that the delays of additional pulses can coincide both with each other and with the main pulses, which, as a result, leads to an increase in the total amplitude and, as a consequence, to a deterioration in the protection efficiency.

For the ML turn with broad-side coupling, we formulated conditions that ensure the decomposition of a USP into crosstalk, an even mode pulse, an additional pulse, and an odd mode pulse, with each of the 4 pulses arriving at the end of the turn with equal time intervals between adjacent pulses. Cross-section parameters of the ML were proven to have an influence on the amplitudes of the main decomposition pulses at the end of the ML. The change in the width of the signal conductor and the thickness of the dielectric substrate were found to have the greatest effect, and the minimum signal amplitude at the output of the line is determined by the amplitude of the additional pulse and the pulses of the even and odd modes of the line.

We achieved a significant improvement of the protective characteristics of the structure with double MR and the asymmetry of excitation (in comparison with a structure with the symmetry of excitation). Using the structure with excitation symmetry, 2 pulses are observed, and with excitation asymmetry, 3 pulses are observed. Thus, without changing the boundary conditions at the ends of the passive conductors, the amplitude of the USP at the output decreases by 14%, and at an SC on one of the passive conductors, it decreases by 31%.

In the structures of a reflection symmetric ML of 2, 3, and 4 cascaded half-turns, additional pulses were revealed in the output signal. It was shown that the values of the delays of the additional pulses are equal to the arithmetic mean value of mode pulse delays in different combinations. However, such pulses may be hidden. It was demonstrated that the amplitude of the output voltage for all circuits is determined precisely by the additional pulse amplitudes. As a result of a comprehensive study of many reflection symmetric ML structures, the method for detecting additional pulses was formulated, which can be useful for studying other structures.

When studying an MF with a passive conductor in the reference plane cutout with different boundary conditions, it was found that the maximum amplitude of the additional pulses is controlled by introducing asymmetry into the MF. Thus, the proximity of the reference conductor made it possible to reduce the amplitude of additional pulses, in comparison with the symmetric structure. Using the same structure as an example, the presence of additional pulses was proved experimentally. It was demonstrated that when the boundary conditions change, additional pulses appear at the ends of the passive conductor. The amplitudes of the additional pulses decrease with increasing the coupling between the conductors. It was shown that delays of additional pulses are determined by a linear combination of per-unit length delays of the line modes multiplied by the line length.

On the example of simulating a turn of the ML with broad-side coupling, it was shown that thanks to an additional pulse, it was possible to increase the attenuation of the USP in the line. Thus, the maximum attenuation of the USP amplitude at the ML output was about 2.3 times before the optimization of the cross-section parameters, and after optimization, it was about 3 times. We note that in the other structures based on modal decomposition, a greater attenuation of the USP is obtained for symmetric structures. Therefore, in the symmetric structure with a single MR, the maximum attenuation of the USP was 2.35 times, and in the asymmetric (under different boundary conditions), it was 2 times. In the symmetric structure of the reflection-symmetric MF, the maximum attenuation of the USP was 4 times, and in the asymmetric structure of the reflection symmetric ML of 2 half-turns, it was 3.78 times. In the asymmetric structure of the reflection-symmetric ML of 3 and 4 half-turns,

the maximum attenuation of the USP was 2.84 times. In the symmetric structure of the MF with a passive conductor in the reference plane cutout, the maximum attenuation of the excitation pulse was 14 times, and in the asymmetric one, it was 10 times. Such results are explained by the fact that in these structures, additional optimization of the parameters of the cross-section was not performed (in contrast to the ML turn with broad-side coupling). However, as shown by the example of the ML turn with broad-side coupling, proper optimization will allow the use of additional pulses to increase the attenuation of a USP in asymmetric structures.

Thus, in symmetric structures or in structures with optimal cross-section parameters, in some cases, additional pulses cannot be observed due to their superposition on each other or on the main pulses. The level of attenuation at the output of such structures will be determined precisely by the maximum amplitude of the superposition of pulses. In this case, it is necessary to detect and separate additional pulses. This will lead to a decrease in maximum amplitude, and as a consequence, to an improvement in the characteristics of such protective devices. Meanwhile, in some cases, the overlapping of bipolar pulses is also possible, which, on the contrary, can improve the characteristics.

Meanwhile, well-known are the results in which various multiconductor structures with modal decomposition, as well as their cascade designs, are considered in the problems of generating a bipolar and unipolar pulse oscillation packet. It can be assumed that with the proper optimization of asymmetric protective structures, after separation of the main and additional pulses, such structures can find application in similar areas, since equal time intervals between all decomposition pulses (both main and additional) can significantly increase the effectiveness of this approach.

Finally, it has been theoretically and experimentally established that additional pulses are a new resource for increasing the efficiency of protective devices with modal decomposition. However, their highest effectiveness is achievable through careful optimization.

4. Conclusions

Thus, for the first time, the paper considers in a unified work the possibility of the appearance of additional pulses in various structures based on modal filtration technology in order to improve protection against USPs. We analyzed an ML with broad-side coupling, structures with MR, reflection symmetric MLs, and an MF with a passive conductor in the reference plane cutout and obtained the following results. First of all, it was shown that the main reason for additional pulses to appear in these structures is the introduction of asymmetry (of cross-section, boundary conditions, and excitation). On the example of simulating a turn of the ML with broad-side coupling, it was shown that the additional pulse allows for an increase in the attenuation of a USP in the line. Next, we demonstrated that the introduction of double MR and asymmetry of excitation improves the protective characteristics of the structure (in contrast to the symmetry-based structure). In the structures of the reflection symmetric ML consisting of 2, 3, and 4 cascaded half-turns, it was shown that the delay values of additional pulses are equal to the arithmetic mean of mode pulse delays in different combinations. Then, on the example of the MF structure with a passive conductor in the reference plane cutout, the presence of additional pulses was proved experimentally. It was illustrated that in some cases, additional pulses cannot be observed because of their overlapping with the main pulses. Therefore, the level of voltage at the output of such structures should be determined precisely by the amplitude of the superposition of pulses. In this case, it is necessary to detect and separate additional pulses, which will lead to a decrease in the output amplitude, and as a result, an improvement in the characteristics of such protective devices. Finally, on the example of the reflection symmetric ML, an improved method for detecting additional pulses was formulated. Thus, it was theoretically and experimentally established that additional pulses are a new resource for increasing the efficiency of protective devices with modal decomposition.

Modal decomposition, which consists in sequential decomposition of the input signal into several modes due to the difference in their propagation speeds, involves the use of symmetrical structures, since they easily provide the desired result thanks to the pseudomatching of each mode propagating

in the structures. However, the present work showed the importance of studying protective devices based on structures not only with symmetry, but also with partial or complete asymmetry. It was demonstrated in an explicit form that certain pulses from the decomposition sequence can include additional pulses. It follows that part of the energy can be separated from the main mode pulses sequence, which means not only an additional distribution of energy over time, but also minimization of the maximum of the mode pulse amplitudes. In addition, the work showed that this maximum amplitude, in some cases, can be determined precisely by the amplitude of the additional pulses (which can either be transmitted from the output of the structure to its load or be reflected to the generator circuit). Meanwhile, all this opens up a wide variety of possibilities. Based on the presented material, three main areas for further research can be distinguished:

1. Optimization of asymmetric structures by evolutionary algorithms according to amplitude and time criteria, which take into account delays of additional mode pulses.
2. Derivation of analytical models for obtaining optimal parameters of additional mode pulses in various structures.
3. Investigation of the possibility of using asymmetric structures not only for protection, but also for solving other problems.

5. Patents

Gazizov, T.R.; Orlov, P.E.; Sharafutdinov V.R.; Kuznetsova-Tadzhibaeva O.M.; Zabolotskij A.M.; Kuksenko S.P.; Buichkin E.N. Printed circuit boards with reserve circuits arrangement method. Russian Federation Patent Application No. 2614156-C2, 23 March 2017.

Nosov, A.V.; Surovtsev, R.S.; Gazizov, T.R. Advanced meander delay line with broad-side coupling that protects against ultrashort pulses. Russian Federation Patent Application No. 2019140941, date of filing 9 December 2020, patent decision date 28 April 2020 (patent decision).

Author Contributions: Conceptualization, T.R.G.; validation, A.M.Z.; investigation, E.B.C., A.O.B., A.V.N., A.V.M. and M.A.S.; writing—original draft preparation, E.B.C., A.O.B., A.V.N., A.V.M. and M.A.S.; writing—review and editing, A.O.B. and T.R.G.; supervision, T.R.G. and A.M.Z.. All authors have read and agreed to the published version of the manuscript.

Funding: The reported study was funded by Russian Science Foundation, project number 19-19-00424 and RFBR, project number 20-37-70020. The experimental research was conducted in the «Impulse» resource sharing center (Russia, Tomsk) with financial support from the Ministry of Science and Higher Education of the Russian Federation under agreement 075-15-2019-1644, project number RFMEFI62119X0029.

Acknowledgments: The authors sincerely appreciate all valuable comments and suggestions from the reviewers, which helped us to improve the quality of the paper.

Conflicts of Interest: The authors declare no conflicts of interest.

References

1. Radasky, W.A.; Baum, C.E.; Wik, M.W. Introduction to the special issue on high-power electromagnetics (HPEM) and intentional electromagnetic interference (IEMI). *IEEE Trans. Electromagn. Compat.* **2004**, *46*, 314–321. [CrossRef]
2. Nitsch, D.; Camp, M.; Sabath, F.; Ter Haseborg, J.-L.; Garbe, H. Susceptibility of Some Electronic Equipment to HPEM Threats. *IEEE Trans. Electromagn. Compat.* **2004**, *46*, 380–389. [CrossRef]
3. Parfenov, Y.V.; Zdoukhov, L.N.; Radasky, W.A.; Ianoz, M. Susceptibility of Some Electronic Equipment to HPEM Threats. *IEEE Trans. Electromagn. Compat.* **2004**, *46*, 404–411. [CrossRef]
4. Kurta, E.; Kovačević, Ž.; Gurbeta, L.; Badnjević, A. Electromagnetic compatibility of medical devices: Effects in everyday healthcare environment. In Proceedings of the 7th Mediterranean Conference on Embedded Computing, Budva, Montenegro, 10–14 June 2018; pp. 1–4. [CrossRef]
5. Mora, N.; Vega, F.; Lugrin, G.; Rachidi, F.; Rubinstein, M. Study and classification of potential IEMI sources. *Syst. Assess. Notes* **2014**, *41*, 92.

6. Weber, T.; Krzikalla, R.; Ter Haseborg, J.L.; Sabath, F. Linear and nonlinear filters suppressing. *IEEE Trans. Electromagn. Compat.* **2004**, *46*, 423–430. [CrossRef]
7. Mojert, C. UWB and EMP susceptiblity of microprocessors and networks. In Proceedings of the 14th International Zurich Symposium on EMC, Zurich, Switzerland, 20–22 February 2001; pp. 47–52.
8. Zhao, Y.; Zhang, G.; Guo, R.; Yang, F. The breakdown characteristics of thermostable insulation materials under high-frequency square waveform. *IEEE Trans. Dielectr. Electr. Insul.* **2019**, *26*, 1073–1080. [CrossRef]
9. Nikoo, M.S.; Hashemi, S.M.-A.; Farzaneh, F. A two-stage DSRD-based high-power nanosecond pulse generator. *IEEE Trans. Plasma Sci.* **2018**, *46*, 427–433. [CrossRef]
10. Egorov, A.B.; Sotnikov, A.M.; Rybalko, I.F. Vozdejstvie moshchnogo elektromagnitnogo izlucheniya na radioelektronnye sredstva. *Proc. of Donetsk Railway Transport Institute* **2012**, *29*, 49–54. (In Russian)
11. Yang, J.; Zhong, H.; Zhang, S.; Tang, Y.; Fan, D. Cascade-gain-switching for generating 3.5-µm nanosecond pulses from monolithic fiber lasers. *IEEE Photonics J.* **2018**, *10*, 1–12. [CrossRef]
12. You, H.; Soma, M. Crosstalk Analysis of Interconnection Lines and Packages in High–Speed Integrated Circuits. *IEEE Trans. Circuits Syst.* **1990**, *8*, 1019–1026. [CrossRef]
13. Bouzidi, Z.; El Idrissi, A.; Rouijaa, H.; Saih, M. Transmission lines modeling approach based on the approximation of Pade. In Proceedings of the 2019 PhotonIcs & Electromagnetics Research Symposium, Rome, Italy, 17–20 June 2019; pp. 4009–4017. [CrossRef]
14. Lim, J.; Lee, S.; Oh, S.; Jeong, J.; Lee, J. Asymmetric coupled lines for common-mode noise suppression in bent differential lines. *Electron. Lett.* **2019**, *55*, 135–136. [CrossRef]
15. Sychev, A.N.; Rudyi, N.Y. Parameters of asymmetric coupled lines with inhomogeneous dielectrics. *Proc. of Tomsk State University of Control Systems and Radioelectronics*. 2018, Volume 21, pp. 7–15. Available online: https://scholar.google.com.hk/scholar?q=doi:10.21293/1818-0442-2018-21-4-1-7-15&hl=en&as_sdt=0,5 (accessed on 5 July 2019). (In Russian) [CrossRef]
16. Park, S.W.; Xiao, F.; Kami, Y. Analytical approach for crosstalk characterization of multiconductor transmission lines using mode decomposition technique in the time domain. *IEEE Trans. Electromagn. Compat.* **2010**, *52*, 436–446. [CrossRef]
17. Chernikova, E.B.; Belousov, A.O.; Gazizov, T.R.; Zabolotsky, A.M. Using reflection symmetry to improve the protection of radio-electronic equipment from ultrashort pulses. *Symmetry* **2019**, *11*. [CrossRef]
18. Gazizov, A.T.; Zabolotsky, A.M.; Gazizov, T.R. UWB pulse decomposition in simple printed structures. *IEEE Trans. Electromagn. Compat.* **2016**, *58*, 1136–1142. [CrossRef]
19. Kuksenko, S.P. Preliminary results of TUSUR University project for design of spacecraft power distribution network: EMC simulation. In *IOP Conference Series Materials Science and Engineering*; IOP Publishing: Bristol, UK, 2019; Volume 560, pp. 1–7. [CrossRef]
20. Thoma, P. State of the art simulation of electromagnetic fields in time domain using the finite integration technique. In Proceedings of the 2019 International Conference on Electromagnetics in Advanced Applications, Cartagena, Colombia, 9–13 September 2019; pp. 0204–0209. [CrossRef]